

EXTENDED CALCULATIONS OF ENERGY LEVELS AND TRANSITION RATES OF ND II-IV IONS FOR APPLICATION TO NEUTRON STAR MERGERS

GEDIMINAS GAIGALAS,¹ DAIJI KATO,^{2,3} PAVEL RYNKUN,¹ LAIMA RADŽIŪTĖ,¹ AND MASAOMI TANAKA⁴

¹*Institute of Theoretical Physics and Astronomy, Vilnius University, Saulėtekio Ave. 3, Vilnius, Lithuania*

²*National Institute for Fusion Science, 322-6 Oroshi-cho, Toki 509-5292, Japan*

³*Department of Advanced Energy Engineering, Kyushu University, Kasuga, Fukuoka 816-8580, Japan*

⁴*Astronomical Institute, Tohoku University, Aoba, Sendai 980-8578, Japan*

(Received January 31, 2019; Revised; Accepted)

ABSTRACT

Coalescence of binary neutron star give rise to electromagnetic emission, kilonova, powered by radioactive decays of r -process nuclei. Observations of kilonova associated with GW170817 provided unique opportunity to study the heavy element synthesis in the Universe. However, atomic data of r -process elements to decipher the light curves and spectral features of kilonova are not fully constructed yet. In this paper, we perform extended atomic calculations of neodymium (Nd, $Z = 60$) to study the impact of accuracies in atomic calculations to the astrophysical opacities. By employing multiconfiguration Dirac-Hartree-Fock and relativistic configuration interaction methods, we calculate energy levels and transition data of electric dipole transitions for Nd II, Nd III, and Nd IV ions. Compared with previous calculations, our new results provide better agreement with the experimental data. The accuracy of energy levels was achieved in the present work 10 %, 3 % and 11 % for Nd II, Nd III and Nd IV, respectively, comparing with the NIST database. We confirm that the overall properties of the opacity are not significantly affected by the accuracies of the atomic calculations. The impact to the Planck mean opacity is up to a factor of 1.5, which affects the timescale of kilonova at most 20%. However, we find that the wavelength dependent features in the opacity are affected by the accuracies of the calculations. We emphasize that accurate atomic calculations, in particular for low-lying energy levels, are important to provide predictions of kilonova light curves and spectra.

Keywords: radiative transfer — opacity — stars: neutron

arXiv:1901.10671v1 [astro-ph.SR] 30 Jan 2019

1. INTRODUCTION

On 2017 August 18, the first observation of gravitational waves (GWs) from neutron star (NS) merger was achieved (GW170817, Abbott et al. (2017a)). In addition to GWs, electromagnetic (EM) counterparts across the wide wavelength range were also observed (Abbott et al. 2017b). In particular, intensive observations of the optical and near-infrared (NIR) counterpart (SSS17a, also known as DLT17ck or AT2017gfo) have been performed and dense photometric and spectroscopic data were obtained (Andreoni et al. 2017; Arcavi et al. 2017; Chornock et al. 2017; Coulter et al. 2017; Cowperthwaite et al. 2017; Díaz et al. 2017; Drout et al. 2017; Evans et al. 2017; Kasliwal et al. 2017; Kilpatrick et al. 2017; Lipunov et al. 2017; McCully et al. 2017; Nicholl et al. 2017; Pian et al. 2017; Shappee et al. 2017; Siebert et al. 2017; Smartt et al. 2017; Soares-Santos et al. 2017; Tanvir et al. 2017; Tominaga et al. 2018; Troja et al. 2017; Utsumi et al. 2017; Valenti et al. 2017). SSS17a shows characteristic properties that are quite different from those of supernovae. The optical light curves decline rapidly while NIR light curves evolve more slowly. The spectra show feature-less, broad-line features implying a high expansion velocity. These properties are broadly consistent with theoretically suggested kilonova or macronova emission from NS mergers (Li & Paczyński 1998; Kulkarni 2005; Metzger et al. 2010).

Kilonova is EM emission powered by radioactive decay energy of r -process nuclei that are newly synthesized in the NS mergers (see Rosswog 2015; Tanaka 2016; Fernández & Metzger 2016; Metzger 2017, for reviews). The timescale, luminosity, and color of the emission are mainly determined by the mass and velocity of the ejecta and opacities in the ejecta. Among r -process elements, lanthanide elements have high optical and NIR opacities (Kasen et al. 2013; Tanaka & Hotokezaka 2013). Therefore, if the ejecta include lanthanide elements, the emission becomes red and faint. On the other hand, if the ejecta is free from lanthanide elements, the emission is blue and bright (Metzger & Fernández 2014; Kasen et al. 2015; Tanaka et al. 2018).

In fact, SSS17a shows both blue and red components, which implies the presence of multiple components with different lanthanide contents. This fact suggests the production of a wide range of r -process elements (Kasen et al. 2017; Tanaka et al. 2017; Rosswog et al. 2017). This is also consistent with the expectation from numerical relativity simulations (see e.g., Shibata et al. 2017; Perego et al. 2017). The ejecta mass to explain the luminosity of SSS17a is about $0.03 - 0.06M_{\odot}$. Although it is still unclear if the r -process yields from NS

mergers are consistent with the solar ratios, NS mergers may be the dominant site for the r -process elements in the Universe (Rosswog et al. 2017; Hotokezaka et al. 2018).

Although the observed properties can be explained by kilonova scenario, physics included in current kilonova simulations is not yet perfect. In particular, atomic data of r -process elements are not complete: so far calculated data are available only for limited number of r -process elements (Kasen et al. 2013; Fontes et al. 2017; Wollaeger et al. 2017; Kasen et al. 2017; Tanaka et al. 2018). Even when the data are available, they are almost entirely based on theoretical calculations, and derived energy levels often deviates from experimental data by up to $\sim 30\%$ (note that experimental data are also insufficient). It is not yet clear if these issues bring systematic impacts to the opacities as well as properties of kilonova.

In this paper, we study impacts of the accuracies in atomic calculations to the opacities by performing extensive, accurate calculations. For this purpose, we choose a lanthanide element, neodymium (Nd, $Z = 60$), which has also been studied by Kasen et al. (2013); Fontes et al. (2017); Tanaka et al. (2018). We focus on singly to triply ionized Nd, for which accurate calculations are possible with the multiconfiguration Dirac-Hartree-Fock method. In Sections 2 and 3, we describe methods and strategies of our atomic calculations. In Section 4, we show and evaluate results of atomic calculations. In Section 5, we show the impact of the accuracy of atomic calculations to the astrophysical opacities. Finally we give summary in Section 6.

2. METHODS

2.1. Computational procedure

The GRASP2K package (Jönsson et al. 2013) is based on the multiconfiguration Dirac-Hartree-Fock (MCDHF) and relativistic configuration interaction (RCI) methods taking into account the transverse photon interaction (Breit interaction) and quantum electrodynamic (QED) corrections (Grant 2007; Fischer et al. 2016).

The MCDHF method used in the present work is based on the Dirac-Coulomb Hamiltonian

$$H_{DC} = \sum_{i=1}^N (c \boldsymbol{\alpha}_i \cdot \mathbf{p}_i + (\beta_i - 1)c^2 + V_i^N) + \sum_{i>j}^N \frac{1}{r_{ij}}(1)$$

where V^N is the monopole part of the electron-nucleus Coulomb interaction, $\boldsymbol{\alpha}$ and β are the 4×4 Dirac matrices, and c is the speed of light in atomic units. The atomic state functions (ASF) were obtained as linear

combinations of symmetry adapted configuration state functions (CSFs)

$$\Psi(\gamma P J M) = \sum_{j=1}^{N_{CSFs}} c_j \Phi(\gamma_j P J M). \quad (2)$$

Here J and M are the angular quantum numbers and P is parity. γ_j denotes other appropriate labeling of the configuration state function j , for example orbital occupancy and coupling scheme. Normally the label γ of the atomic state function is the same as the label of the dominant CSF. The CSFs are built from products of one-electron Dirac orbitals. Based on a weighted energy average of several states, the so called extended optimal level (EOL) scheme (Dyall et al. 1989), both the radial parts of the Dirac orbitals and the expansion coefficients were optimized to self-consistency in the relativistic self-consistent field procedure. Note that accurate calculations with the MCDHF method is much more difficult for neutral atoms than ions (Grant 2007), we focus on ionized Nd.

For these calculation, we used the spin-angular approach (Gaigalas & Rudzikas 1996; Gaigalas et al. 1997) which is based on the second quantization in coupled tensorial form, on the angular momentum theory in three spaces (orbital, spin, and quasispin) and on the reduced coefficients of fractional parentage. It allow us to study configurations with open f -shells without any restrictions.

In subsequent RCI calculations the Breit interaction

$$H_{\text{Breit}} = - \sum_{i < j}^N \left[\alpha_i \cdot \alpha_j \frac{\cos(\omega_{ij} r_{ij}/c)}{r_{ij}} + (\alpha_i \cdot \nabla_i)(\alpha_j \cdot \nabla_j) \frac{\cos(\omega_{ij} r_{ij}/c) - 1}{\omega_{ij}^2 r_{ij}/c^2} \right] \quad (3)$$

was included in the Hamiltonian. The photon frequencies ω_{ij} , used for calculating the matrix elements of the transverse photon interaction, were taken as the difference of the diagonal Lagrange multipliers associated with the Dirac orbitals (McKenzie et al. 1980). In the RCI calculation the leading QED corrections, self-interaction and vacuum polarization, were also included.

In the present calculations, the ASFs were obtained as expansions over jj -coupled CSFs. To provide the LSJ labeling system, the ASFs were transformed from a jj -coupled CSF basis into an LSJ -coupled CSF basis using the method provided by Gaigalas et al. (2017).

2.2. Computation of transition parameters

The evaluation of radiative transition data (transition probabilities, oscillator strengths) between two states:

$\gamma' P' J' M'$ and $\gamma P J M$, built on different and independently optimized orbital sets is non-trivial. The transition data can be expressed in terms of the transition moment, which is defined as

$$\langle \Psi(\gamma P J) \| \mathbf{T} \| \Psi(\gamma' P' J') \rangle = \sum_{j,k} c_j c'_k \langle \Phi(\gamma_j P J) \| \mathbf{T} \| \Phi(\gamma'_k P' J') \rangle, \quad (4)$$

where \mathbf{T} is the transition operator. For electric dipole and quadrupole (E1 and E2) transitions there are two forms of the transition operator: the length (Babushkin) and velocity (Coulomb) forms, which for the exact solutions of the Dirac-equation give the same value of the transition moment (Grant 1974). The quantity dT , characterizing the accuracy of the computed transition rates, is defined as

$$dT = \frac{|A_l - A_v|}{\max(A_l, A_v)}, \quad (5)$$

where A_l and A_v are transition rates in length and velocity forms.

The calculation of the transition moment breaks down to the task of summing up reduced matrix elements between different CSFs. The reduced matrix elements can be evaluated using standard techniques assuming that both left and right hand CSFs are formed from the same orthonormal set of spin-orbitals. This constraint is severe, since a high-quality and compact wave function requires orbitals optimized for a specific electronic state, see for example (Fritzsche & Grant 1994). To get around the problems of having a single orthonormal set of spin-orbitals, the wave function representations of the two states: $\gamma' P' J' M'$ and $\gamma P J M$, were transformed in such way that the orbital sets became biorthonormal (Olsen et al. 1995). Standard methods were then used to evaluate the matrix elements of the transformed CSFs.

3. SCHEMES OF THE CALCULATIONS

3.1. Active space construction

Summary of the MCDHF and RCI calculations for each ion is given in Table 1. The description, which explains in what way these calculations were done is given below. As a starting point DHF calculations were performed in the EOL scheme for the states of the ground configuration. The wave functions from these calculations were taken as the initial ones to calculate even and odd states of multireference (MR) configurations. The set of orbitals belonging to these MR configurations are referred to as 0 layer (OL).

Table 1. Summary of active space construction

Ion	Ground conf.	MR set		Active space	Number of levels		N_{CSFs}	
		Even	Odd		Even	Odd	Even	Odd
Strategies A, B.1								
Nd II	$4f^4 6s$	$4f^4 6s, 4f^4 5d$	$4f^3 5d^2, 4f^4 6p$	$\{8s, 8p, 7d, 6f, 5g\}$	3 890	2 998	24 568	23 966
		$4f^3 5d 6p, 4f^3 6s 6p$	$4f^3 5d 6s$					
Additional configuration in Strategy B.2								
		$4f^4 6d, 4f^3 5d 7p$	$4f^4 7p, 4f^4 5f$	$\{10s, 10p, 9d, 8f, 7g\}$	1 039	1 013	468 652	468 029
		$4f^4 7s$						
Strategy C								
		$4f^4 6s, 4f^4 5d$	$4f^3 5d^2, 4f^4 6p$	$\{8s, 8p, 7d, 6f, 5g\}$	3 270	2 813	188 357	113 900
		$4f^3 5d 6p, 4f^3 6s 6p$	$4f^3 5d 6s$					
Strategies A, B								
Nd III	$4f^4$	$4f^4, 4f^3 6p$	$4f^3 5d, 4f^3 6s$	$\{9s, 9p, 8d, 7f, 7g, 7h\}$	1 020	468	400 440	259 948
		$4f^2 5d^2, 4f^2 5d 6s$						
Strategy C								
		$4f^4, 4f^3 6p$	$4f^3 5d, 4f^3 6s$	$\{10s, 10p, 9d, 8f, 7g, 7h\}$	747	706	844 637	559 294
		$4f^2 5d^2, 4f^2 5d 6s$	$4f^3 6d, 4f^3 7s$					
		$4f^3 5f, 4f^3 7p$						
Strategy C with 5p,5s								
		$4f^4, 4f^3 6p$	$4f^3 5d, 4f^3 6s$	$\{10s, 10p, 9d, 8f, 7g, 7h\}$	747	706	900 904	586 850
		$4f^2 5d^2, 4f^2 5d 6s$	$4f^3 6d, 4f^3 7s$					
		$4f^3 5f, 4f^3 7p$						
Strategy A								
Nd IV	$4f^3$	$4f^2 5d, 4f^2 6s$	$4f^3, 4f^2 6p$	$\{9s, 9p, 8d, 7f, 7g, 7h, 7i\}$	131	110	33 825	26 590
Strategy B								
		$4f^2 5d, 4f^2 6s$	$4f^3, 4f^2 6p$	$\{9s, 9p, 8d, 7f, 7g, 7h\}$	1 068	465	1 445 481	587 774
		$5p^5 4f^3 5d$	$5p^5 4f^4$					
Strategy B with 5s								
		$4f^2 5d, 4f^2 6s$	$4f^3, 4f^2 6p$	$\{9s, 9p, 8d, 7f, 7g, 7h\}$	1 068	465	1 474 463	603 827
		$5p^5 4f^3 5d$	$5p^5 4f^4$					

Unless stated otherwise, the inactive core of each ion used in present calculations is [Xe]. The CSF expansions for states of each parity were obtained by allowing single (S) and double (SD) substitutions from the MR configurations up to active orbital sets (see Table 1). The configuration space was increased step by step with increasing the number of layers (L). The orbitals of previous layers were held fixed and only the orbitals of the newest layer were allowed to vary. For example, the

scheme used to increase the active spaces of the CSFs for Nd III ion (in Strategy A) is presented below:

$$\begin{aligned}
 AS_{0L} &= \{6s, 6p, 5d\}, \\
 AS_{1L} &= AS_{0L} + \{7s, 7p, 6d, 5f, 5g\}, \\
 AS_{2L} &= AS_{1L} + \{8s, 8p, 7d, 6f, 6g, 6h\}, \\
 AS_{3L} &= AS_{2L} + \{9s, 9p, 8d, 7f, 7g, 7h\}.
 \end{aligned}$$

The MCDHF calculations were followed by RCI calculations, including the Breit interaction and leading QED effects. The number of CSFs in the final even and odd

state expansions distributed over the different J symmetries is presented in Table 1.

3.2. Strategies for Nd II ion

Four strategies were tested for Nd II ion. All of them were computed in the active space described in the Table 1. For the **Strategy A** a starting point DHF calculations were performed in the EOL scheme for the states of the ground configuration $4f^46s$. The wave functions from these calculations were taken as the initial ones to calculate even and odd states of MR configurations. The set of orbitals belonging to these MR configurations are referred to as 0 layer (0L). The active space were generated as is presented in the Table 1.

For **Strategy B.1** the starting point was computation of the wave functions for the core $4f^46s$. Wave functions were computed in the neutral system of Nd I - ground state $4f^46s^2$. Then AS_{0L} was computed: the core shells were frozen and only $5d$ and $6p$ shells of the configurations of MR listed in Table 1 were computed. Even and odd states were computed together. Later, wave functions were optimized separately for states of different parities in the AS_{1L} . AS_{1L} and the next active space were generated by SD substitutions from shells $4f, 5d, 6p, 6s$.

In the **Strategy B.2** the configurations of the Rydberg states listed in Table 1 were added to the multireference list; therefore, the first active set included subshells bigger by one principal quantum number. Then the first active space of the **Strategy B.2** was $AS_{1L} = AS_{0L} + \{8s, 8p, 7d, 6f, 5g\}$.

In **Strategy C** computation were performed for each configuration separately. For configurations $4f^46s$, $4f^46p$ and $4f^45d$ SD substitutions were allowed from $4f^4nl$ (where $l = s, p, d$) shells in to the $AS_{0L,1L}$ and S to the AS_{2L} . For configurations $4f^35d6s$, $4f^35d6p$, $4f^36s6p$, and $4f^35d^2$ only S substitutions were allowed. Radial wavefunctions up to $4f$ orbital was taken from ground configuration for these configurations. The Breit interaction and leading QED effects are included in RCI computations.

3.3. Strategies for Nd III ion

After AS_{0L} the even and odd states were calculated separately in **Strategy A**. For the Nd III ion calculations the **Strategy B** was also applied. **Strategy B** differs from **Strategy A** in the fact that virtual orbitals for odd parity were taken from even parity states instead of varying them in layer 1, and higher layers.

In **Strategy C** as compared to **Strategy A** additional configurations: $4f^36d$, $4f^37s$ (odd parity) and $4f^35f$, $4f^37p$ (even parity) were added to the MR set.

In **Strategy C with $5p, 5s$** just RCI calculations were performed. The wavefunctions were taken from **Strategy C** and configurations with S substitutions from $5p$ and $5s$ shells to $\{6s, 6p, 5d, 4f\}$ shells were added additionally in the active space.

3.4. Strategies for Nd IV ion

In **Strategy B** as compared to **Strategy A** additional configurations: $4p^54f^4$ (odd parity) and $4p^54f^35d$ (even parity) were added to the MR set. The AS for even and odd parities were constructed in such way: SD substitutions were allowed from the $4f, 5d, 6s, 6p$ shells up to active orbital sets and S substitution from $5p$ shell to $\{6s, 6p, 5d, 4f\}$ shells. In **Strategy B with $5s$** just RCI calculations were performed. The wave functions were taken from **Strategy B** and configurations with S substitutions from $5s$ shells to $\{6s, 6p, 5d, 4f\}$ shells were added additionally in the active space.

4. RESULTS

4.1. Nd II

A part of all computed excitation energies for Nd II are listed in Table 2. These data were compared with NIST database by evaluating relative difference $\Delta E/E = (E_{NIST} - E)/E_{NIST}$. Energy levels computed with Breit interaction and QED effects are presented in columns marked by *. Levels with changed notations are given in Table 3.

Note that the energy levels of Nd II are also provided by Wyart (2010). They interpreted 596 levels of odd configurations ($4f^35d6s$, $4f^35d^2$, $4f^36s^2$, $4f^46p$ and $4f^5$) in semi-empirical way following the Racah-Slater parametric method, by using the Cowan computer codes. In their method, radial parameters obtained in a least-squares fit were compared with Hartree-Fock (HFR) *ab initio* integrals. In such a way, obtained energy levels naturally have very small disagreement with NIST values, therefore are not presented in this paper.

Energy levels for each configurations are compared with NIST in the figure 1. Among different strategies, **Strategy C** AS_{2L} gives the best agreement with the NIST database. Averaged difference between our computed data and NIST presented values is 10 %. This is significant improvement as compared with **Strategy A** AS_{2L} (blue in Figure 1), which was used to compute the opacity of the neutron star mergers in Tanaka et al. (2018). The averaged difference with the NIST is 22 % in **Strategy A** AS_{2L} . For the comparison with the NIST, expression $\overline{\Delta E/E} = \frac{\sum |\Delta E_i/E_i|}{N}$ was used, where N is the number of compared levels.

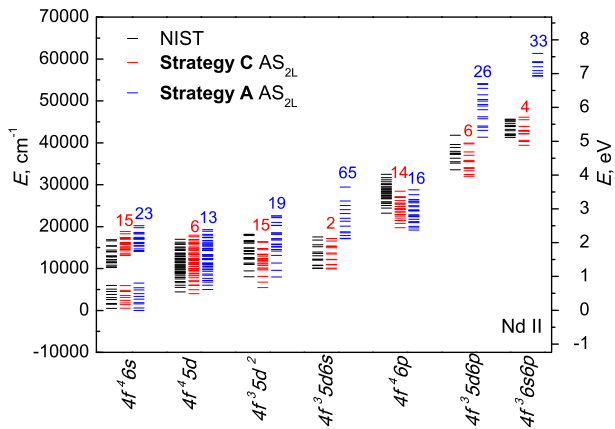


Figure 1. Energy levels for configurations of Nd II are compared with data of NIST. Black color is representing NIST data, next column of levels in red is our computed energy levels in **Strategy C** AS_{2L} , blue color data are based on **Strategy A** AS_{2L} (used in Tanaka et al. 2018). Number on top of red and blue column is averaged disagreement in % for levels of each configuration comparing with NIST database.

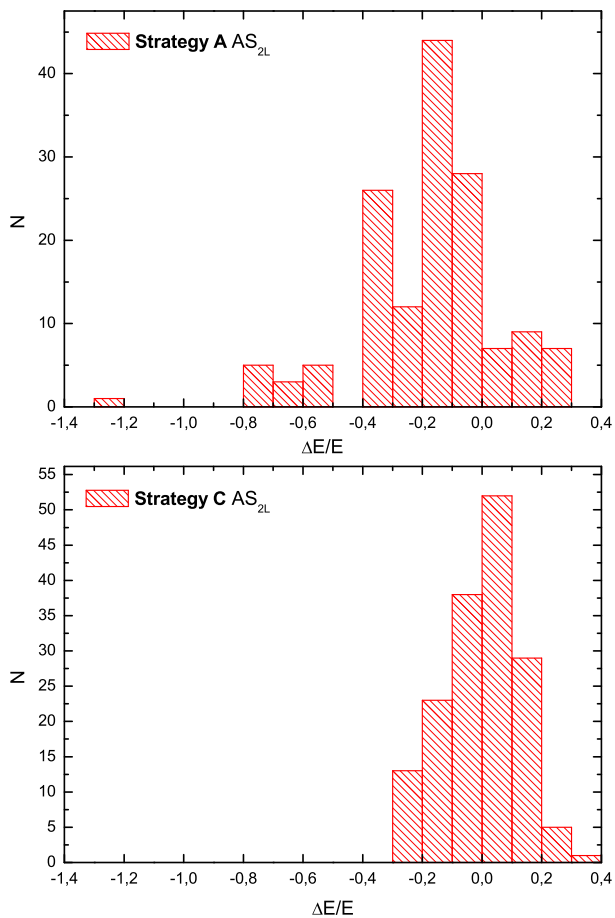


Figure 2. Distribution of the energy levels (N) according the disagreement with NIST database for Nd II using **Strategy A** and **Strategy C** in AS_{2L} .

The figure 2 shows distribution of the energy levels number over relative difference comparing with the NIST for **Strategy A** in active space AS_{2L} . For the strategies **A**, **B.1** and **B.2** in all active spaces the view of the distribution is very similar. In case of **Strategy C** in AS_2 (see figure 2) normal distribution with smaller $\Delta E/E$ range is observed.

Energy data computed in **Strategy C** at layer 2 are given in machine readable Table 9. This includes number, label, J and P values, and energy value. Transitions data obtained from **Strategy C** at layer 2 are given in machine readable Table 10. This includes identification of upper and lower levels in LSJ coupling, transition energy, wavelength, line strength, weighted oscillator strength, and transitions probabilities in length form.

4.2. Nd III

Results of the energy levels for Nd III obtained applying **Strategies: A, B C, and C with 5p, 5s** are compared with the NIST database and presented in Table 4. Among different strategies, **Strategy C with 5p, 5s** gives the best agreement with the NIST database although the number of available levels is smaller than in the case of Nd II. All the energy levels and transition data obtained from this strategy are given the machine readable Tables 11 and 12. Figure 3 shows the comparison of the energy levels with the NIST database. The averaged difference between our calculations with **Strategy C with 5p, 5s** AS_{3L} and the NIST data is 3 %. For comparison, the difference for the case of **Strategy B** AS_{2L} , which as used by Tanaka et al. (2018), is 5 % (blue in Figure 3).

Results of the energy levels obtained from **Strategy C with 5p, 5s** are also compared with those by Dzuba et al. (2003) in Table 5. They evaluated energy levels and lifetimes of configurations $4f^4$, $4f^35d$ using relativistic Hartree-Fock and configuration-interaction (RCI) codes as well as a set of computer codes written by Cowan (1981). Note that Zhang, Z. G. et al. (2002) also presented low-lying odd energy levels (below $33\,000\text{ cm}^{-1}$) belonging to the configurations: $4f^35d$ and $4f^36s$. To compute these energy levels, the HFR, described and coded by Cowan (1981) but modified with the inclusion of core-polarization effects was used. It should be mentioned, however, that core-core correlation was not included in energy levels computations.

Disagreement between our data obtained applying **Strategy C** and **Strategy C with 5p, 5s** as compared to recommended data by NIST is slightly larger than disagreement between data computed by Dzuba et al. (2003) (Cowan) as compared to recommended data by NIST. In this paper we present the lowest 1453 levels

Table 2. Computations of energy values (in cm^{-1}) of Nd II by increase of the active space performed applying **Strategy A**, **Strategy B.1**, **Strategy B.2**, and **Strategy C** and their comparison with NIST data base (in %). With the '*' energy levels were computed with Breit interaction and QED effects are presented.

Config.	Term	J	NIST	Strategy A		Strategy B.1			Strategy B.2			Strategy C		
				AS _{1L} /	AS _{2L}	AS _{1L} /AS _{2L}	/AS _{2L} *	/AS _{3L}	AS _{1-2L} /AS _{2-3L} /AS _{3-4L}	AS _{1L} */AS _{2L} *				
$4f^4(^5I)6s$	6I	7/2	0.000											
	6I	9/2	513.330	-14 /	-9	-16/	-10 /	-2 /	-10	-9 /	-9 /	-9	-6 /	-7
	6I	11/2	1470.105	-5 /	-3	-6/	-3 /	8 /	-3	-0 /	0 /	-3	5 /	4
$4f^4(^5I)6s$	4I	9/2	1650.205	-13 /	-8	-15/	-9 /	-3 /	-8	-8 /	-7 /	-8	-8 /	-8
$4f^4(^5I)6s$	6I	13/2	2585.460	-5 /	-3	-4/	-3 /	9 /	-3	1 /	1 /	-3	6 /	6
$4f^4(^5I)6s$	4I	11/2	3066.755	-9 /	-6	-10/	-6 /	2 /	-6	-4 /	-4 /	-6	-1 /	-2
$4f^4(^5I)6s$	6I	15/2	3801.930	-5 /	-4	-5/	-4 /	8 /	-4	0 /	0 /	-4	6 /	6
$4f^4(^5I)5d$	6L	11/2	4437.560	-13 /	-7	-38/	-3 /	2 /	-3	-2 /	-3 /	1	4 /	9
$4f^4(^5I)6s$	4I	13/2	4512.495	-9 /	-6	-9/	-6 /	0 /	-6	-4 /	-3 /	-6	0 /	0
$4f^4(^5I)6s$	6I	17/2	5085.640	-6 /	-5	-6/	-5 /	7 /	-5	-1 /	-1 /	-5	6 /	6
$4f^4(^5I)5d$	6L	13/2	5487.655	-10 /	-5	-30/	-2 /	1 /	-2	-1 /	-1 /	1	6 /	10
$4f^4(^5I)6s$	4I	15/2	5985.580	-9 /	-7	-9/	-7 /	4 /	-7	-4 /	-4 /	-7	1 /	1
$4f^4(^5I)5d$	6K	9/2	6005.270	-12 /	-7	-36/	-4 /	-3 /	-4	-5 /	-5 /	-2	-6 /	-1
$4f^4(^5I)5d$	6L	15/2	6637.430	-8 /	-4	-24/	-1 /	3 /	-1	0 /	0 /	0	7 /	10
$4f^4(^5I)5d$	6K	11/2	6931.800	-10 /	-6	-31/	-3 /	-1 /	-3	-3 /	-3 /	-2	-3 /	1
$4f^4(^5I)5d$	6I	7/2	7524.735	-24 /	-19	-50/	-17 /	-16 /	-17	-19 /	-19 /	-15	-16 /	-1
$4f^4(^5I)5d$	6L	17/2	7868.910	-7 /	-3	-20/	-1 /	4 /	-1	1 /	1 /	0	7 /	10
$4f^4(^5I)5d$	6K	13/2	7950.075	-9 /	-5	-27/	-3 /	1 /	-3	-3 /	-3 /	-2	-2 /	2
$4f^3(^4I)5d^2(^3F)$	$^6M^o$	13/2	8009.810	0 /	-12	-7/	-11 /	-6 /	-14	-7 /	-10 /	-14	32 /	32
$4f^4(^5I)5d$	6I	9/2	8420.320	-21 /	-16	-43/	-14 /	-12 /	-14	-15 /	-16 /	-13	-13 /	-9
$4f^4(^5I)5d$	6G	3/2	8716.445	-20 /	-15	-42/	-13 /	-12 /	-13	-16 /	-16 /	-13	-14 /	-11
	6G	5/2	8796.365	-23 /	-17	-46/	-15 /	-14 /	-15	-19 /	-19 /	-15	-17 /	-14
$4f^4(^5I)5d$	6K	15/2	9042.760	-8 /	-5	-24/	-3 /	2 /	-3	-2 /	-2 /	-2	0 /	3
$4f^4(^5I)5d$	6L	19/2	9166.210	-6 /	-3	-17/	-1 /	5 /	-1	1 /	1 /	-1	7 /	10
$4f^4(^5I)5d$	6G	7/2	9198.395	-24 /	-18	-46/	-16 /	-15 /	-16	-19 /	-19 /	-15	-17 /	-14
$4f^4(^5I)5d$	6I	11/2	9357.910	-18 /	-14	-39/	-12 /	-10 /	-12	-13 /	-13 /	-11	-10 /	-7
$4f^3(^4I)5d^2(^3F)$	$^6M^o$	15/2	9448.185	-1 /	-12	-9/	-12 /	-6 /	-14	-8 /	-11 /	-14	29 /	29
$4f^4(^5I)5d$	6H	5/2	9674.835	-28 /	-22	-55/	-20 /	-20 /	-30	-24 /	-25 /	-19	-23 /	-19
$4f^3(^4I)5d(^5L)6s$	$^6L^o$	11/2	10054.195	-71 /	-50	-73/	-77 /	73 /	-79	-73 /	-75 /	-79	1 /	1
$4f^3(^4I)5d(^5K)6s$	$^6K^o$	9/2	10091.360	-70 /	-51	-71/	-75 /	-101/	-77	-71 /	-73 /	-77	-1 /	0
$4f^4(^5I)5d$	6K	17/2	10194.805	-8 /	-5	-21/	-3 /	2 /	-3	-2 /	-2 /	-3	1 /	3
$4f^4(^5F)6s$	6F	1/2	10256.040	-37 /	-37	-38/	-37 /	-36 /	-35	-37 /	-35 /	-35	-28 /	-28
$4f^4(^5I)5d$	6I	13/2	10337.100	-17 /	-13	-35/	-11 /	-8 /	-11	-12 /	-12 /	-11	-8 /	-6
$4f^4(^5F)6s$	6F	3/2	10439.225	-37 /	-36	-37/	-48 /	-36 /	-35	-36 /	-34 /	-35	-28 /	-27
$4f^4(^5I)5d$	6L	21/2	10516.790	-6 /	-3	-15/	-1 /	5 /	-1	0 /	0 /	-2	7 /	9
$4f^4(^5I)5d$	6H	7/2	10666.780	-25 /	-20	-36/	-19 /	-17 /	-18	-11 /	-11 /	-8	-19 /	-16
$4f^3(^4I)5d(^5K)6s$	$^6K^o$	11/2	10720.295	-67 /	-82	-82/	-82 /	-69 /	-75	-69 /	-80 /	-75	-3 /	-2
$4f^4(^5F)6s$	6F	5/2	10786.775	-36 /	-36	-37/	-50 /	-35 /	-34	-35 /	-47 /	-34	-27 /	-27

Table 3. NIST recommended energy levels notations changed by the authors for the Nd II.

NIST label	Our label
$4f^3(4I^*)5d(5K^*)6s\ 6L^*$	$4f^3(4I^*)5d(5L^*)6s\ 6L^*$
$4f^2(4I^*)5d(5K^*)6s\ 6I^*$	$4f^3(4I^*)5d(5I^*)6s\ 6I^*$

of energy spectra and transitions between these states whereas Dzuba et al. (2003) presented only small part of the spectra (88 levels). This paper aims at presenting a more complete set of atomic data for astrophysics. This is clearly reflected in the figure 3 where energy levels for each configurations at different strategies are presented and compared with only a few levels of configuration $4f^4$ and $4f^35d$ available in the NIST.

Table 4. Comparison of energy levels with NIST database (in %) of Nd III by increase of the active space performed applying **Strategies: A, B, C, and C with 5p, 5s**. States marked by subscript * in term column are without term identification in the NIST database.

Config.	Term	J	NIST	Strategy A			Strategy B			Strategy C			Strategy C (5p,5s)		
				AS _{1L} /	AS _{2L} /	AS _{3L}	AS _{1L} /	AS _{2L} /	AS _{3L}	AS _{1L} /	AS _{2L} /	AS _{3L}	AS _{1L} /	AS _{2L} /	AS _{3L}
$4f^4$	5I	4	0.0												
		5	1137.8	8.8/	8.5/	8.4	8.7/	8.5/	8.4	8.8/	8.5/	8.4	6.1/	5.9/	5.7
		6	2387.6	7.9/	7.7/	7.7	7.9/	7.7/	7.7	7.9/	7.8/	7.7	5.4/	5.3/	5.2
		7	3714.9	7.0/	7.0/	7.0	7.0/	7.0/	7.0	7.1/	7.1/	7.0	4.7/	4.7/	4.6
$4f^3(4I)5d$	$^5K^o$	8	5093.3	6.2/	6.2/	6.3	6.2/	6.2/	6.3	6.3/	6.4/	6.3	4.0/	4.1/	4.1
		5	15262.2	7.2/	11.6/	7.4	6.8/	6.4/	6.8	7.5/	7.0/	6.8	1.4/	1.1/	0.9
		6	16938.1	7.0/	11.0/	7.1	6.7/	6.3/	6.6	7.4/	6.8/	6.6	1.9/	1.5/	1.3
$4f^3(4I)5d$	$^5I^o$	7	18656.3	6.6/	10.2/	6.7	6.4/	6.0/	6.3	7.0/	6.4/	6.2	2.1/	1.7/	1.5
$4f^3(4I)5d$	$^5I^o$	4	18883.7	-2.7/	2.1/	-1.2	-3.5/	-2.8/	-1.8	-2.3/	-1.7/	-1.7	0.5/	0.9/	0.9
$4f^3(4I)5d$	$^5H^o$	3	19211.0	-5.3/	-0.5/	-3.8	-6.2/	-5.1/	-4.3	-5.0/	-4.2/	-4.2	-3.7/	-2.8/	-2.8
		4	20144.3	-3.2/	1.3/	-1.8	-3.9/	-3.1/	-2.4	-2.9/	-2.3/	-2.3	-2.3/	-1.6/	-1.6
$4f^3(4I)5d$	$^5I^o$	5	20388.9	-1.9/	2.5/	-0.6	-2.6/	-2.1/	-1.1	-1.5/	-1.1/	-1.1	0.5/	0.9/	0.9
$4f^3(4I)5d$	$^5K^o$	8	20410.9	6.1/	9.4/	6.2	5.9/	5.5/	5.8	6.4/	5.9/	5.7	2.0/	1.7/	1.5
$4f^3(4I)5d$	$^5H^o$	5	21886.8	-2.5/	1.6/	-1.3	-3.1/	-2.4/	-1.8	-2.2/	-1.7/	-1.7	-1.6/	-1.0/	-1.1
$4f^3(4I)5d$	$^5I^o$	6	22047.8	-1.3/	2.7/	-0.2	-1.9/	-1.4/	-0.6	-0.9/	-0.5/	-0.6	0.6/	0.9/	0.9
$4f^3(4I)5d$	$^5K^o$	9	22197.0	5.5/	8.6/	5.6	5.4/	5.0/	5.2	5.8/	5.4/	5.2	1.9/	1.6/	1.4
$4f^3(4I)5d$	$^5I^o$	7	22702.9	-1.0/	2.9/	0.2	-1.5/	-1.1/	-0.3	-0.6/	-0.2/	-5.8	0.6/	0.9/	0.9
$4f^3(4I)5d$	$^5H^o$	6	23819.3	-1.8/	1.9/	-0.7	-2.3/	-1.8/	-1.2	-1.5/	-1.1/	-1.1	-1.2/	-0.7/	-0.7
$4f^3(4I)5d$	o*	7	24003.2												
$4f^3(4I)5d$	$^5I^o$	8	24686.4	-1.3/	2.3/	-0.2	-1.8/	-1.4/	-0.6	-0.9/	-0.6/	-0.6	1.4/	1.6/	1.6
$4f^3(4I)5d$	o*	6	26503.2												
$4f^3(4I)5d$	$^3K^o$	8	27391.4	-0.4/	3.0/	0.8	-0.8/	-0.4/	0.4	-0.1/	0.4/	0.5	-0.9/	-0.4/	-0.3
$4f^3(4F)5d$	o*	3	27569.8												
$4f^3(4F)5d$	$^5H^o$	3	27788.2	-10.3/	-6.9/	-8.9	-10.7/	-10.2/	-9.3	-9.9/	-9.4/	-9.2	-6.7/	-6.2/	-6.1
		4	28745.3	-10.1/	-6.8/	-8.8	-10.5/	-10.0/	-9.2	-9.7/	-9.2/	-9.1	-6.6/	-6.2/	-6.1
$4f^3(4F)5d$	o*	5	29397.3												
$4f^3(4F)5d$	$^5H^o$	5	30232.3	-8.9/	-5.7/	-7.6	-9.3/	-8.8/	-8.0	-8.5/	-8.0/	-7.9	-6.0/	-5.5/	-5.4
		6	31394.6	-7.5/	-4.4/	-6.1	-7.8/	-7.3/	-6.5	-7.2/	-6.6/	-6.4	-4.8/	-4.2/	-5.0
		7	32832.6	-7.4/	-4.4/	-6.1	-7.8/	-7.3/	-6.5	-7.1/	-6.5/	-6.4	-5.0/	-4.4/	-4.3

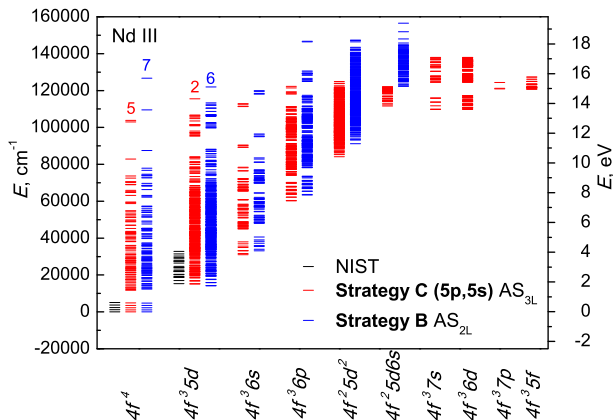


Figure 3. Energy levels for configurations of Nd III are compared with data of NIST. Black color is representing NIST data, next column of levels in red is our computed energy levels in **Strategy C (5p,5s) AS_{3L}**, blue color data are based on **Strategy B AS_{2L}**. Number on top of red and blue column is averaged disagreement in % for levels of each configuration comparing with NIST database.

4.3. Nd IV

Results of the energy levels of **Strategies A and B** are presented and compared with the NIST database in Table 6. The best agreement with the NIST database is obtained for **Strategy B with 5s**. The energy levels are shown and compared with a few levels of configuration $4f^3$ available in the NIST in Figure 4. The averaged difference is 11 % for **Strategy B with 5s** while it is 17 % for **Strategy A** in active space AS_{1L} .

For Nd IV ion, several experiments and analysis by semi-empirical methods have been performed. The emission spectrum produced by vacuum spark sources was observed in the vacuum ultraviolet on two normal-incidence spectrographs. 550 lines have been identified as transitions from 85 (out of 107 possible) levels of $4f^25d$ to 37 (out of 41 possible) levels of $4f^3$. The method and codes of Cowan were used to predict the spectral ranges of the strong transitions in the spectra Nd IV in the beginning of paper series (Wyart et al. 2006).

Later Wyart et al. (2007) used the same experiment to observe and classify 1426 lines. In total, 41 levels of $4f^3$ configuration were reported. For deriving their energy levels with the diagonalization code RCG, the input Hartree-Fock radial integrals including relativistic corrections, treated as parameters (HFR parameters), were scaled according to earlier results on the neighbouring ions spectra. Altogether 111 odd parity and 121 even parity of configurations $4f^3$, $4f^26p$, $5p^54f^4$, $4f^25d$, $4f^26s$, and $5p^54f^35d$ levels were established. Their op-

timized values were calculated with the ELCALC code (Radziemski et al. 1970).

Then Wyart et al. (2008) performed a parametric fit of levels energies for $4f^3$ configuration, previously obtained in the experiment (Wyart et al. 2007). Dzuba et al. (2003) did computation in the same way as for Nd III (see subsection 4.2). This included only 72 levels of configurations $4f^3$ and $4f^25d$. In Table 7, the energy levels obtained applying **Strategy B with 5s** are compared with the experimental values by (Wyart et al. 2007) and semi-empirical values by Dzuba et al. (2003).

In addition to the energy levels, transition data can also be compared with experimental data and semi-empirical calculations (Table 8). Our results on the transition wavelengths show good agreement with the experimental data by Wyart et al. (2007). As shown in Figure 5, the agreement in the wavelength is within 20 % for the most transitions.

We also confirmed a nice agreement in the transition probabilities. Table 8 and Figure 6 show transition probabilities for strongest transitions computed by Wyart et al. (2007). Our and their results agree within a factor of 2. Note that semi-empirical calculations have uncertainties. Using the the same HFR method combined with parametric least-squares fits to the same experimental data with Wyart et al. (2007), Yoca & Quinet (2014) have computed and presented transition probabilities (only with $\log gf \geq -1.0$), oscillator strengths and radiative lifetimes in bigger multiconfiguration expansions than Wyart et al. (2007). Their results are systematically different, and those by Yoca & Quinet (2014) in fact show a slightly better agreement with ours as shown in the bottom panel of Figure 6.

5. IMPACT TO THE OPACITIES

We calculate bound-bound opacities using our results to study the impact of the accuracy in the atomic calculations. By following previous works on NS mergers (Kasen et al. 2013; Barnes & Kasen 2013; Tanaka & Hotokezaka 2013; Tanaka et al. 2014, 2018), we use the formalism of expansion opacity (Karp et al. 1977; Eastman & Pinto 1993; Kasen et al. 2006):

$$\kappa_{\text{exp}}^{\text{bb}}(\lambda) = \frac{1}{\rho ct} \sum_l \frac{\lambda_l}{\Delta\lambda} (1 - e^{-\tau_l}). \quad (6)$$

Here, ρ and t represent density and time after the merger. The summation is taken over all the transitions in a wavelength bin ($\Delta\lambda$), and λ_l and τ_l are the transition wavelength and the Sobolev optical depth for each

Table 5. Comparison of energy levels from present (**Strategy C with 5p, 5s**) and other theoretical computations with NIST database (in %) of Nd III. States marked by subscript * in term column are without term identification in the NIST database.

Config.	Term	J	NIST	Present		Dzuba et al. (2003)		
				AS_{3L}		Cowan	RCI	
$4f^4$	5I	4	0.0	0		0		0
		5	1137.8	1073/	5.7	1137/	0.1	1162/ -2.1
		6	2387.6	2264/	5.2	2397/	-0.4	2471/ -3.5
		7	3714.9	3543/	4.6	3743/	-0.8	3898/ -4.9
		8	5093.3	4885/	4.1	5148/	-1.1	5414/ -6.3
$4f^3(^4I)5d$	$^5K^o$	5	15262.2	15128/	0.9	14742/	3.4	15357/ -0.6
		6	16938.1	16721/	1.3	16338/	3.5	17380/ -2.6
		7	18656.3	18383/	1.5	18000/	3.5	19485/ -4.4
$4f^3(^4I)5d$	$^5I^o$	4	18883.7	18714/	0.9	18467/	2.2	20284/ -7.4
$4f^3(^4I)5d$	$^5H^o$	3	19211.0	19753/	-2.8	19427/	-1.1	20946/ -9.0
		4	20144.3	20465/	-1.6	20189/	-0.2	21926/ -8.8
$4f^3(^4I)5d$	$^5I^o$	5	20388.9	20208/	0.9	20006/	1.9	21254/ -4.2
$4f^3(^4I)5d$	$^5K^o$	8	20410.9	20105/	1.5	19725/	3.4	21666/ -6.1
$4f^3(^4I)5d$	$^5H^o$	5	21886.8	22119/	-1.1	21866/	0.1	22167/ -1.3
$4f^3(^4I)5d$	$^5I^o$	6	22047.8	21845/	0.9	21672/	1.7	22664/ -2.8
$4f^3(^4I)5d$	$^5K^o$	9	22197.0	21882/	1.4	21503/	3.1	21919/ 1.3
$4f^3(^4I)5d$	$^5I^o$	7	22702.9	22499/	0.9	22244/	2.0	26537/ -16.9
$4f^3(^4I)5d$	$^5H^o$	6	23819.3	23992/	-0.7	23733/	0.4	24076/ -1.1
$4f^3(^4I)5d$	o*	7	24003.2					
$4f^3(^4I)5d$	$^5I^o$	8	24686.4	24301/	1.6	24158/	2.1	27396/ -11.0
$4f^3(^4I)5d$	o*	6	26503.2					
$4f^3(^4I)5d$	$^3K^o$	8	27391.4	27465/	-0.3			
$4f^3(^4F)5d$	o*	3	27569.8					
$4f^3(^4F)5d$	$^5H^o$	3	27788.2	29494/	-6.1	28824/	-3.7	
		4	28745.3	30506/	-6.1	29872/	-3.9	
$4f^3(^4F)5d$	o*	5	29397.3					
$4f^3(^4F)5d$	$^5H^o$	5	30232.3	31852/	-5.4	31117/	-2.9	
		6	31394.6	32961/	-5.0	32054/	-2.1	
		7	32832.6	34234/	-4.3	33391/	-1.7	

transition. The Sobolev optical depth τ_l is expressed as

$$\tau_l = \frac{\pi e^2}{m_e c} f_l n_l t \lambda_l = \frac{\pi e^2}{m_e c} \left(\frac{n \lambda_l t}{g_0} \right) g_l f_l e^{-E_l/kT}, \quad (7)$$

where g_l , E_l , and f_l are the statistical weight and the energy of the lower level of the transition and the oscillator strength of the transition, respectively. For the oscillator strength, we use results computed with the length (Babushkin) form. For the number density in the lower level of the transition (n_l), the Boltzmann distribution is assumed, i.e., $n_l = (g_l/g_0)n \exp(-E_l/kT)$, where g_0 is

the statistical weight for the ground level. The number density of each ion n is calculated under the assumption of local thermodynamic equilibrium by using the Saha equation. In this paper, pure Nd gas is assumed. We use all the calculated transitions to evaluate the opacity without any selection based on the transition strengths, which was applied in full radiative transfer simulations (Tanaka et al. 2017).

We find that overall properties of opacities are not dramatically affected by the accuracies of the atomic

Table 6. Comparison of energy levels with NIST database (in %) of Nd IV by increase of the active space performed applying **Strategies: A, B, and B with 5s**. State marked by subscript * in term column is without term identification in the NIST database.

Config.	Term	J	NIST	Strategy A			Strategy B			Strategy B (5s)		
				AS _{1L} /	AS _{2L} /	AS _{3L}	AS _{1L} /	AS _{2L} /	AS _{3L}	AS _{1L} /	AS _{2L} /	AS _{3L}
$4f^3$	$4I^o$	9/2	0									
		11/2	[1880]	6.8/	6.5/	6.4	6.9/	6.8/	6.7	7.2 /	7.1 /	7.0
		13/2	[3860]	5.6/	5.4/	5.3	5.8/	5.8/	5.7	6.1 /	6.1 /	6.0
$4f^3$	$4F^o$	15/2	[5910]	4.7/	4.6/	4.6	4.9/	5.0/	5.0	5.2 /	5.3 /	5.3
		3/2	[11290]	-27.8/	-27.0/	-26.6	-20.3/	-19.2/	-18.6	-17.6/	-16.4 /	-15.8
		5/2	[12320]	-24.8/	-24.2/	-23.8	-17.9/	-16.9/	-16.4	-15.3/	-14.4 /	-13.8
$4f^3$	$2H2^o$	9/2	[12470]	-14.7/	-12.5/	-11.3	-12.8/	-10.4/	-9.4	-12.0/	-9.5 /	-8.5
$4f^3$	$4F^o$	7/2	[13280]	-22.3/	-21.6/	-21.2	-16.1/	-15.2/	-14.6	-13.7/	-12.8 /	-12.3
$4f^3$	$4S^o$	3/2	[13370]	-20.2/	-16.8/	-16.5	-15.6/	-12.1/	-11.6	-13.3/	-9.8 /	-9.3
$4f^3$	$4F^o$	9/2	[14570]	-18.3/	-17.6/	-17.1	-13.2/	-12.1/	-11.6	-11.3/	-10.2 /	-9.7
$4f^3$	$2H2^o$	11/2	[15800]	-9.6/	-7.8/	-6.8	-8.4/	-6.3/	-5.5	-7.8 /	-5.7 /	-4.9
$4f^3$	$4G^o$	5/2	[16980]	-29.6/	-28.1/	-27.8	-21.7/	-20.2/	-19.6	-18.6/	-17.1 /	-16.5
$4f^3$	o^*	7/2	[17100]									
$4f^3$	$4G^o$	7/2	[18890]	-23.6/	-22.3/	-22.0	-16.9/	-15.5/	-14.9	-14.3/	-12.9 /	-12.3
		9/2	[19290]	-16.6/	-27.0/	-26.7	-22.1/	-20.6/	-20.0	-19.7/	-18.3 /	-17.7
$4f^3$	$2K^o$	13/2	[19440]	-17.7/	-15.0/	-14.2	-15.1/	-12.2/	-11.4	-13.9/	-11.1 /	-10.3
$4f^3$	$4G^o$	11/2	[21280]	-22.2/	-21.0/	-20.8	-15.9/	-14.6/	-14.2	-13.4/	-12.2 /	-11.7
$4f^3$	$2K^o$	15/2	[21430]	-16.1/	-13.7/	-12.9	-13.6/	-11.0/	-10.3	-12.5/	-9.9 /	-9.2

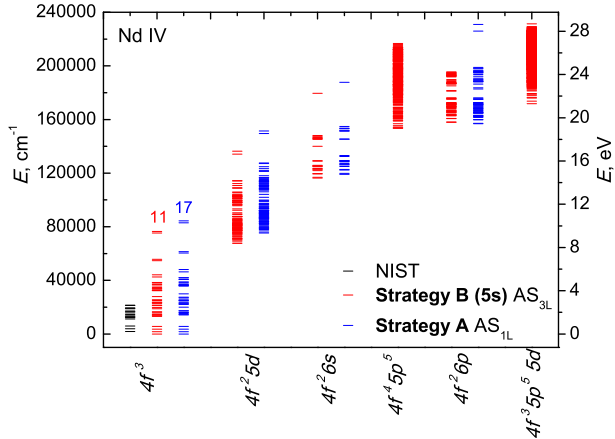


Figure 4. Energy levels for configurations of Nd IV are compared with data of NIST. Black color is representing NIST data, next column of levels in red is our computed energy levels in **Strategy B (5s) AS_{3L}**, blue color data are based on **Strategy A AS_{1L}**. Number on top of red and blue column is averaged disagreement in % for levels of each configuration comparing with NIST database.

calculations. Left panels in figure 7 shows the expansion opacities calculated by using transition data of Nd

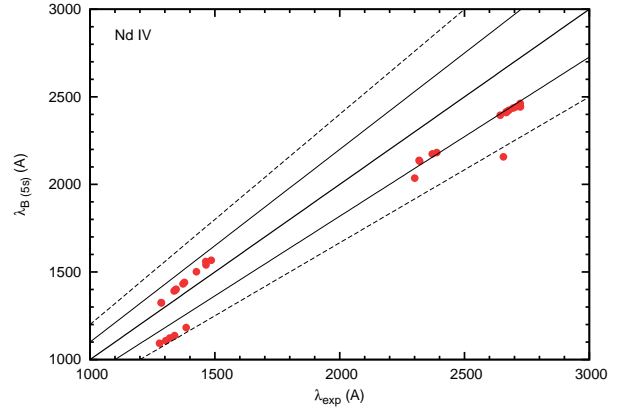


Figure 5. Comparison of transition wavelengths for Nd IV between our results from **Strategy B with 5s** and experimental data by [Wyart et al. \(2007\)](#). The thick line corresponds to the perfect agreement while thin solid and dashed lines correspond to 10% and 20 % deviation.

II, Nd III, and Nd IV. The temperature is assumed to be 5000 K, 10000 K, and 15000 K for Nd II, Nd III, and Nd IV, respectively. The density is $1 \times 10^{-13} \text{ g cm}^{-3}$ and time after the merger is set to be 1 day. Overall opacity values and wavelength dependence are quite

Table 7. Comparison of energy levels from present (**Strategy B with 5s**) and other theoretical computations with NIST database (in %) and with the experiment [Wyart et al. \(2007\)](#) (in %) of Nd IV. State marked by subscript * in term column is without term identification in the NIST database.

Config.	Term	J	NIST	Exp.	Present			Dzuba et al. (2003)					
					AS _{3L}			Cowan			RCI		
$4f^3$	$4I^o$	9/2	0	0	0			0			0		
		11/2	[1880]	1897.11	1749/	7.0/	7.8	1879/	0.1/	1.0	1945/	-3.5/	-2.5
		13/2	[3860]	3907.43	3627/	6.0/	7.2	3890/	-0.8/	0.4	4049/	-4.9/	-3.6
$4f^3$	$4F^o$	15/2	[5910]	5988.51	5596/	5.3/	6.6	5989/	-1.3/	0.0	6267/	-6.0/	-4.7
		3/2	[11290]	11698.49	13076/	-15.8/	-11.8	13294/	-17.8/	-13.6	12490/	-10.6/	-6.8
$4f^3$	$4F^o$	5/2	[12320]	12747.94	14022/	-13.8/	-10.0	14333/	-16.3/	-12.4	13545/	-9.9/	-6.3
$4f^3$	$2H2^o$	9/2	[12470]	12800.29	13536/	-8.5/	-5.8	13272/	-6.4/	-3.7	14522/	-16.5/	-13.5
$4f^3$	$4F^o$	7/2	[13280]	13719.82	14911/	-12.3/	-8.7	15249/	-14.8/	-11.1	14622/	-10.1/	-6.6
$4f^3$	$4S^o$	3/2	[13370]	13792.49	14617/	-9.3/	-6.0	15153/	-13.3/	-9.9	14452/	-8.1/	-4.8
$4f^3$	$4F^o$	9/2	[14570]	14994.87	15979/	-9.7/	-6.6	16334/	-12.1/	-8.9	16183/	-11.1/	-7.9
$4f^3$	$2H2^o$	11/2	[15800]	16161.53	16581/	-4.9/	-2.6	16456/	-4.2/	-1.8	18142/	-14.8/	-12.3
$4f^3$	$4G^o$	5/2	[16980]	17707.17	19780/	-16.5/	-11.7						
$4f^3$	o^*	7/2	[17100]	17655.11									
$4f^3$	$4G^o$	7/2	[18890]	19540.80	21218/	-12.3/	-8.6						
		9/2	[19290]	19969.79	22709/	-17.7/	-13.7						
$4f^3$	$2K^o$	13/2	[19440]	20005.22	21445/	-10.3/	-7.2						
$4f^3$	$4G^o$	11/2	[21280]	22047.39	23768/	-11.7/	-7.8						
$4f^3$	$2K^o$	15/2	[21430]	22043.77	23398/	-9.2/	-6.1						

similar for different atomic calculations. The red lines show the best results in this paper while blue lines show the previous results used by [Tanaka et al. \(2018\)](#).

The behaviors of the opacity are also similar for different temperature. Right panels show the Planck mean opacities calculated for different temperatures by keeping the density and time to be the same. The Planck mean opacity from different atomic calculations agree with each other within a factor of 1.5. Since the timescale of the kilonova emission scales as $\kappa^{0.5}$ ([Rosswog 2015](#); [Tanaka 2016](#); [Fernández & Metzger 2016](#); [Metzger 2017](#)), this level of differences does not significantly affect the timescale of kilonova (smaller than $\sim 20\%$) compared with those expected from differences in temperature and abundances.

With a close look, however, the wavelength dependent opacities show some differences. The most notable difference is the feature around 4000 Å in the case of Nd II. The new GRASP2K calculations with a better accuracy show a bump while the old GRASP2K calculations and HULLAC calculations do not, making a difference in the opacity by a factor of 2. Interestingly, [Kasen et al. \(2013\)](#) also showed that this part of the opacity is af-

ected by the optimization in the atomic calculations: the peak is located near 5000 Å in their opt1 case while the peak is weaker in their opt2 and opt3 cases. The expansion opacities presented by [Fontes et al. \(2017\)](#) also show a peak around 4000 Å, which is close to our new results.

We find that the difference between our new and previous opacities is caused by the lower energy levels of $4f^35d^2$ and $4f^35d6s$ configurations in our new calculations (Figure 1). Figure 8 shows the number of strong transitions which fulfill $g_l f_l \exp(-E_l/kT) > 10^{-5}$ at $T = 5000$ K. The numbers of transition are separated according to the lower level configuration. The number of strong transition from the levels of $4f^35d^2$ and $4f^35d6s$ configuration is enhanced around 4500 Å in our new calculations (**Strategy C AS_{2L}**). Since the energy of these configurations are overestimated in our previous calculations (**Strategy A AS_{2L}**, Figure 1), the bump structure in the new calculations seems more realistic. This demonstrates the importance of accurate calculations for lower energy levels to predict spectra of kilonova.

Table 8. Computed transitions data of Nd IV in the **Strategies B with 5s** at AS_{3L} and compared with the experimental wavelength λ_{exp} (in Å) and computed transitions probabilities A_{SE} (in s^{-1}) by [Wyart et al. \(2007\)](#).

Upper	Lower	Strategies B with 5s						Wyart et al. (2007)		Yoca & Quinet (2014)
		A_I	A_V	dT	λ	A_{SE}	λ_{exp}	A_{SE}		
$4f^2(^3H)6p^4I$	4.5	$4f^2(^3H)5d^2H$	4.5	5.26E+8	4.40E+8	0.16	1107.72(15.0)	4.04E+8	1303.32	3.89E+8
$4f^2(^1I)5d^2K$	7.5	$4f^3^2L$	8.5	9.32E+7	1.24E+8	0.25	1540.16(-5.1)	1.64E+8	1464.73	1.47E+8
$4f^2(^3H)6p^4I$	5.5	$4f^2(^3H)6s^4H$	5.5	2.04E+8	1.91E+8	0.06	2412.27(9.5)	1.96E+8	2666.70	1.94E+8
$4f^2(^3H)6p^4I$	4.5	$4f^2(^3H)6s^4H$	3.5	1.92E+8	1.61E+8	0.16	2410.31(9.6)	1.97E+8	2666.70	1.96E+8
$4f^2(^1G)5d^2I$	6.5	$4f^3^2K$	7.5	6.85E+7	8.99E+7	0.24	1559.66(-6.6)	1.28E+8	1463.34	1.14E+8
$4f^2(^3F)5d^4H$	5.5	$4f^3^4I$	6.5	3.78E+7	5.67E+7	0.33	1324.01(-3.0)	8.92E+7	1285.61	6.48E+7
$4f^2(^3F)5d^4H$	4.5	$4f^3^4I$	5.5	4.11E+7	6.19E+7	0.34	1325.17(-3.1)	1.04E+8	1285.38	7.55E+7
$4f^2(^3H)5d^4H$	3.5	$4f^3^4I$	4.5	7.27E+7	1.03E+8	0.29	1401.4(-4.2)	1.29E+8	1344.74	1.17E+8
$4f^2(^3H)6p^4I$	4.5	$4f^2(^3H)5d^4K$	5.5	1.01E+9	8.05E+8	0.20	1123.17(14.9)	7.61E+8	1319.25	7.29E+8
$4f^2(^3H)6p^4G$	5.5	$4f^2(^3H)6s^4H$	6.5	1.55E+8	1.65E+8	0.06	2157.57(18.8)	2.17E+8	2656.02	2.16E+8
$4f^2(^1I)6p^2I$	5.5	$4f^2(^1I)6s^2I$	5.5	2.30E+8	2.17E+8	0.06	2443.54(10.3)	1.70E+8	2723.51	1.86E+8
$4f^2(^3H)6p^4H$	4.5	$4f^2(^3H)6s^4H$	5.5	2.02E+8	2.07E+8	0.02	2416.08(9.5)	2.00E+8	2670.03	2.04E+8
$4f^2(^3H)6p^4H$	3.5	$4f^2(^3H)6s^4H$	4.5	1.95E+8	2.00E+8	0.02	2423.25(9.5)	1.99E+8	2678.00	
$4f^2(^3H)5d^4H$	5.5	$4f^3^4I$	6.5	7.27E+7	1.04E+8	0.30	1391.9(-4.1)	1.29E+8	1336.98	1.00E+8
$4f^2(^3H)5d^4I$	7.5	$4f^3^4I$	7.5	4.69E+7	8.18E+7	0.43	1432.37(-4.4)	9.05E+7	1372.20	7.44E+7
$4f^2(^1I)6p^2I$	5.5	$4f^2(^1I)6s^2I$	6.5	1.16E+8	1.20E+8	0.03	2443.59(10.3)	1.17E+8	2723.51	1.22E+8
$4f^2(^3H)6p^4H$	4.5	$4f^2(^3H)6s^2H$	4.5	1.38E+8	1.30E+8	0.05	2436.05(9.6)	1.27E+8	2694.71	
$4f^2(^3H)5d^4H$	4.5	$4f^3^4I$	5.5	7.02E+7	9.97E+7	0.30	1397.63(-4.1)	1.24E+8	1342.01	1.10E+8
$4f^2(^3H)6p^2I$	6.5	$4f^2(^3H)6s^2H$	5.5	3.29E+8	2.88E+8	0.13	2174(8.3)	2.84E+8	2370.51	2.94E+8
$4f^2(^3F)6p^4D$	3.5	$4f^2(^3F)6s^4F$	4.5	2.86E+8	2.88E+8	0.01	2394.67(9.4)	2.89E+8	2643.03	2.93E+8
$4f^2(^1I)6p^2K$	6.5	$4f^2(^1I)6s^2I$	6.5	7.68E+7	7.75E+7	0.01	2181.33(8.7)	8.11E+7	2388.79	1.26E+8
$4f^2(^3H)6p^4I$	7.5	$4f^2(^3H)5d^4K$	8.5	1.34E+9	1.07E+9	0.20	1093.02(14.5)	6.16E+8	1278.41	6.63E+8
$4f^2(^3H)6p^2I$	6.5	$4f^2(^3H)5d^2K$	7.5	7.92E+8	6.02E+8	0.24	1182.67(14.6)	4.37E+8	1385.21	4.89E+8
$4f^2(^3H)6p^4I$	6.5	$4f^2(^3H)6s^4H$	5.5	4.95E+8	4.43E+8	0.10	2132.31(8.1)	3.65E+8	2320.43	4.09E+8
$4f^2(^3F)6p^4G$	5.5	$4f^2(^3F)6s^4F$	4.5	5.00E+8	4.56E+8	0.09	2137.32(7.8)	4.15E+8	2318.07	3.98E+8
$4f^2(^3H)6p^2I$	5.5	$4f^2(^3H)6s^4H$	4.5	1.90E+7	1.56E+7	0.18	2035.66(11.5)	3.96E+8	2300.68	4.16E+8
$4f^2(^3H)6p^4H$	5.5	$4f^2(^3H)5d^4H$	5.5	2.85E+8	2.39E+8	0.16	1136.61(15.1)	1.54E+8	1338.62	1.03E+8
$4f^2(^1I)5d^2K$	6.5	$4f^3^2L$	7.5	6.41E+7	8.42E+7	0.24	1501.86(-5.3)	1.27E+8	1426.05	1.14E+8
$4f^2(^3H)6p^4I$	4.5	$4f^2(^3H)6s^4H$	4.5	1.78E+8	1.65E+8	0.07	2443.44(9.8)	1.71E+8	2708.43	1.70E+8
$4f^2(^3H)6p^4H$	5.5	$4f^2(^3H)6s^2H$	5.5	1.16E+8	1.10E+8	0.06	2462.26(9.6)	1.18E+8	2723.34	1.23E+8
$4f^2(^3H)5d^4I$	6.5	$4f^3^4I$	6.5	4.40E+7	7.69E+7	0.43	1440.32(-4.5)	8.54E+7	1378.09	6.95E+7
$4f^2(^1I)5d^2I$	6.5	$4f^3^2K$	7.5	3.75E+7	4.99E+7	0.25	1566.59(-5.4)	7.14E+7	1485.64	6.43E+7

Figure 9 shows the cumulative number of states (CNS) for $4f^35d^2$ and $4f^35d6s$ configurations as a function of excitation energies. It is noted that the number of states takes the statistical-weight (degeneracy) of each level, *i. e.* $2J + 1$, into account. The CNS for the whole energy levels obtained by calculations with GRASP2K and HULLAC is compared in the figure. The CNS of the new calculations gets rising at a lower energy and has larger values than those of the previous calculations with

GRASP2K and HULLAC, indicating that the larger number of states falls into the lower energy region with the new calculations. Since the Boltzmann distribution is assumed for the number density in the lower levels of transitions, it is predicted that the number of strong transitions from the levels of $4f^35d^2$ and $4f^35d6s$ configurations becomes larger with the new calculations as depicted in Fig. 8. This is more remarkable for $4f^35d6s$ configuration as in the CNS. The CNS of the new cal-

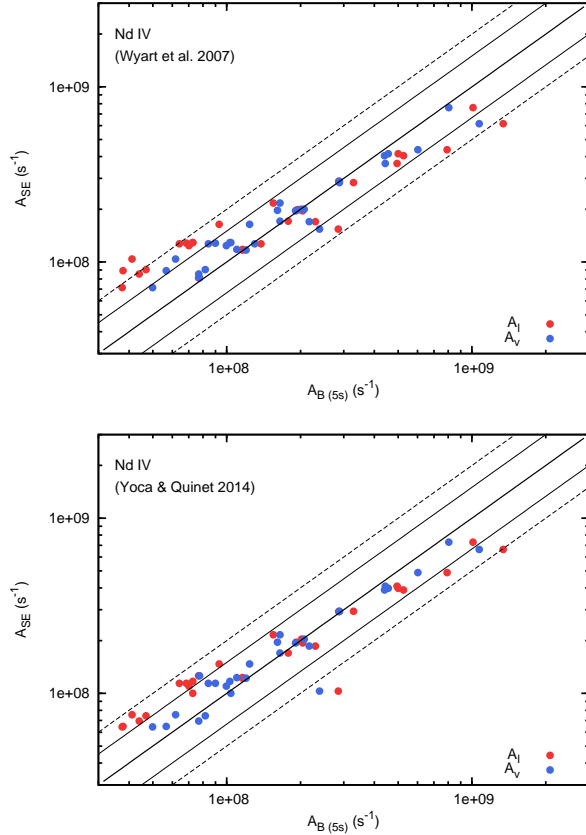


Figure 6. Comparison of transition probability for Nd IV. The top and bottom panels show comparison between our results from **Strategy B with 5s** and semi-empirical results by Wyart et al. (2007) and by Yoca & Quinet (2014), respectively. The thick line corresponds to the perfect agreement while thin solid and dashed lines correspond to the deviation by a factor of 1.5 and 2.0, respectively. Red and blue points show the values calculated with the length (Babushkin) and velocity (Coulomb) forms, respectively.

calculations is compared also with those of NIST and the semi-empirical results by Wyart (2010). Overall agreement is good at low energies convincing accuracy of our new calculations. Only exception is the semi-empirical results for $4f^35d^2$ configuration which overshoot significantly at high energies. Reasons of this discrepancy are yet to be investigated.

Another notable difference is a feature around 1000 \AA : the opacities in our new calculations are suppressed. This is due to the inclusion of highly excited energy levels in the previous calculations (both GRASP2K and HULLAC). Therefore, the opacities in the ultraviolet wavelengths depends on the choice of the configurations included in the calculations. However, if configurations with sufficiently high energy ($E \sim 10 - 15 \text{ eV}$) are in-

cluded, such a difference appears only in the far ultraviolet wavelength, and thus, does not affect observable features.

6. SUMMARY

We presented extensive atomic calculations of neodymium and studied impact of accuracies in the calculations to the astrophysical opacities. The extended search of electron correlation effect inclusion strategies is presented in this work for the three Nd ions (Nd II, III and IV). In total, 6 000, 1 453, 1 533 levels are presented for Nd II, Nd III and Nd IV respectively, and E1 type transitions between these levels were computed. Exclusive accuracy is achieved for atomic energy spectra results. Compared with NIST database, the averaged relative differences are 10 %, 3 %, and 11 % for Nd II, Nd III, and Nd IV, respectively.

Using our new results, we calculated expansion opacities used in radiative transfer simulations for kilonova, radioactively-powered EM emission from NS merger. We found that the overall opacities values and their wavelength dependence are not very sensitive to the accuracies of the calculations. The Planck mean opacities from our previous and new atomic calculations agree within a factor of 1.5. This confirms the validity of previous studies on kilonova.

However, some wavelength dependent features are affected by the accuracy of atomic calculations. In particular, the low-lying energy levels ($E < 2 - 3 \text{ eV}$) can affect the opacities and even produce a bump in a certain wavelength range. Our results highlight importance of accurate atomic calculations for low-lying energy levels to accurately predict the spectra of kilonova.

This research was funded by a grant (No. S-LJB-18-1) from the Research Council of Lithuania. This research was also supported by JSPS Bilateral Joint Research Project. Computations presented in this paper were performed at the High Performance Computing Center “HPC Sauletekis” of the Faculty of Physics at Vilnius University and with Cray XC30 and XC50 at Center for Computational Astrophysics, National Astronomical Observatory of Japan. DK is grateful to the support by NINS program of Promoting Research by Networking among Institutions (Grant Number 01411702). MT is supported by the NINS program for cross-disciplinary science study, Inoue Science Research Award from Inoue Foundation for Science, and the Grant-in-Aid for Scientific Research from JSPS (15H02075, 16H02183) and MEXT (17H06363).

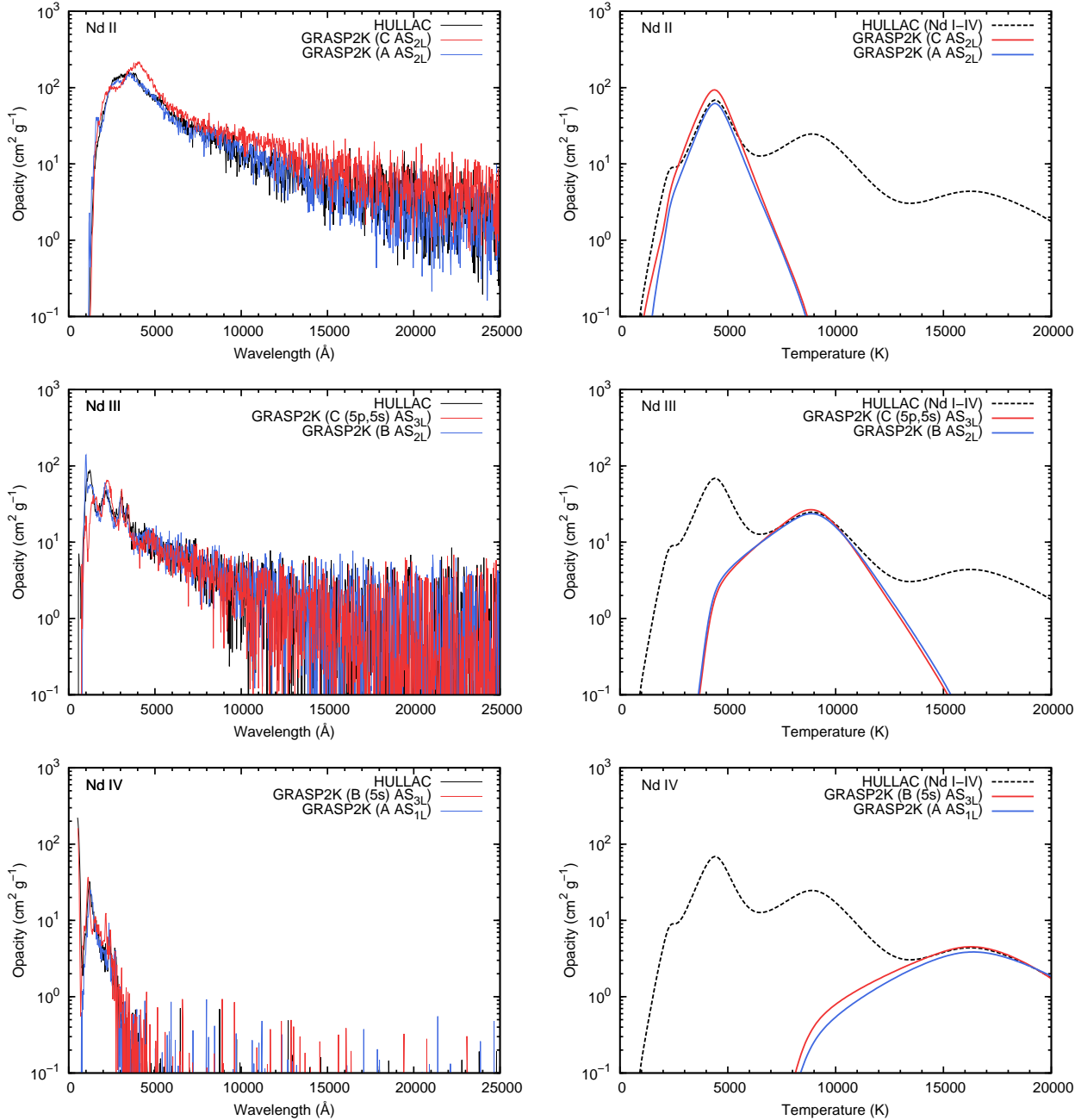


Figure 7. Opacities for Nd II (top), Nd III (middle), and Nd IV (bottom) ions. The left panels show the expansion opacities calculated with $T = 5000$ K, 10000 K, and 15000 K for Nd II, Nd III, and Nd IV, respectively. The density and time are assumed to be $\rho = 1 \times 10^{-13}$ g cm $^{-3}$ and $t = 1$ day after the merger, respectively. The right panels show Planck mean opacities for various temperatures. The dashed curve shows the Planck mean opacities calculated with atomic data for Nd I-IV calculated with the HULLAC code (Tanaka et al. 2018).

REFERENCES

- Abbott, B. P., Abbott, R., Abbott, T. D., et al. 2017a, *Physical Review Letters*, 119, 161101
- . 2017b, *ApJL*, 848, L12
- Andreoni, I., Ackley, K., Cooke, J., et al. 2017, *PASA*, 34, e069
- Arcavi, I., Hosseinzadeh, G., Howell, D. A., et al. 2017, *Nature*, 551, 64
- Barnes, J., & Kasen, D. 2013, *ApJ*, 775, 18
- Chornock, R., Berger, E., Kasen, D., et al. 2017, *ApJL*, 848, L19

Table 9. Energy levels (in cm^{-1}) relative to the ground state for the lowest states of Nd II.

No.	label	J	P	E
1	$4f^4(\frac{5}{1}I)6s\ ^6I$	7/2	+	0.00
2	$4f^4(\frac{5}{1}I)6s\ ^6I$	9/2	+	547.86
3	$4f^4(\frac{5}{1}I)6s\ ^6I$	11/2	+	1404.36
4	$4f^4(\frac{5}{1}I)6s\ ^4I$	9/2	+	1789.52
5	$4f^4(\frac{5}{1}I)6s\ ^6I$	13/2	+	2425.58
6	$4f^4(\frac{5}{1}I)6s\ ^4I$	11/2	+	3120.96
7	$4f^4(\frac{5}{1}I)6s\ ^6I$	15/2	+	3564.21
8	$4f^4(\frac{5}{1}I)5d\ ^6L$	11/2	+	4019.24
9	$4f^4(\frac{5}{1}I)6s\ ^4I$	13/2	+	4506.07
10	$4f^4(\frac{5}{1}I)6s\ ^6I$	17/2	+	4789.43
11	$4f^4(\frac{5}{1}I)5d\ ^6L$	13/2	+	4941.03
12	$4f^3(\frac{4}{1}I)5d^2(\frac{3}{2}F)\ ^6M$	13/2	-	5477.69
13	$4f^4(\frac{5}{1}I)6s\ ^4I$	15/2	+	5940.53
14	$4f^4(\frac{5}{1}I)5d\ ^6L$	15/2	+	5965.42
15	$4f^4(\frac{5}{1}I)5d\ ^6K$	9/2	+	6065.11
16	$4f^3(\frac{4}{1}I)5d^2(\frac{3}{2}F)\ ^6M$	15/2	-	6750.71
17	$4f^4(\frac{5}{1}I)5d\ ^6K$	11/2	+	6881.31
18	$4f^4(\frac{5}{1}I)5d\ ^6L$	17/2	+	7078.84
19	$4f^4(\frac{5}{1}I)5d\ ^6K$	13/2	+	7802.57
20	$4f^3(\frac{4}{1}I)5d^2(\frac{3}{2}F)\ ^6M$	17/2	-	8147.61

NOTE— Table 9 is published in its entirety in the machine-readable format. Part of the values are shown here for guidance regarding its form and content.

- Coulter, D. A., Foley, R. J., Kilpatrick, C. D., et al. 2017, *Science*, 358, 1556
- Cowan, R. 1981, *The Theory of Atomic Structure and Spectra* (University of California Press, Berkeley, CA)
- Cowperthwaite, P. S., Berger, E., Villar, V. A., et al. 2017, *ApJL*, 848, L17
- Díaz, M. C., Macri, L. M., Garcia Lambas, D., et al. 2017, *ApJL*, 848, L29
- Drout, M. R., Piro, A. L., Shappee, B. J., et al. 2017, *Science*, 358, 1570
- Dyall, K., Grant, I., Johnson, C., Parpia, F., & Plummer, E. 1989, *Computer Physics Communications*, 55, 425
- Dzuba, V. A., Safronova, U. I., & Johnson, W. R. 2003, *Phys. Rev. A*, 68, 032503
- Eastman, R. G., & Pinto, P. A. 1993, *ApJ*, 412, 731
- Evans, P. A., Cenko, S. B., Kennea, J. A., et al. 2017, *Science*, 358, 1565
- Fernández, R., & Metzger, B. D. 2016, *Annual Review of Nuclear and Particle Science*, 66, 23
- Fischer, C. F., Godefroid, M., Brage, T., Jönsson, P., & Gaigalas, G. 2016, *Journal of Physics B: Atomic, Molecular and Optical Physics*, 49, 182004
- Fontes, C. J., Fryer, C. L., Hungerford, A. L., et al. 2017, arXiv:1702.02990, arXiv:1702.02990
- Fritzsche, S., & Grant, I. 1994, *Physics Letters A*, 186, 152
- Gaigalas, G., Fischer, C., Rynkun, P., & Jönsson, P. 2017, *Atoms*, 5, 6
- Gaigalas, G., & Rudzikas, Z. 1996, *Journal of Physics B: Atomic, Molecular and Optical Physics*, 29, 3303
- Gaigalas, G., Rudzikas, Z., & Fischer, C. F. 1997, *Journal of Physics B: Atomic, Molecular and Optical Physics*, 30, 3747
- Grant, I. P. 1974, *Journal of Physics B: Atomic and Molecular Physics*, 7, 1458

Table 10. Transition energies ΔE (in cm^{-1}), transition wavelengths λ (in \AA), line strengths S (in a.u.), weighted oscillator strengths gf and transition rates A (in s^{-1}) for E1 transitions of Nd II ion. All transition data are in length form. dT is the relative difference of the transition rates in length and velocity form as given by Eq. (5).

upper	lower	ΔE	λ	S	gf	A	dT
$4f^3(4I)5d^2(3F)^6L_{11/2}$	$4f^3(4I)5d^5K6p^6L_{11/2}$	22745	4396.48	4.593E+00	3.173E-01	9.127E+06	0.050
$4f^3(4I)5d^2(3F)^6L_{11/2}$	$4f^3(4I)5d^5L6p^6L_{11/2}$	23391	4275.02	1.001E+01	7.115E-01	2.164E+07	0.154
$4f^3(4I)5d^2(3F)^6L_{11/2}$	$4f^3(4I)5d^5K6p^6K_{11/2}$	24959	4006.51	7.628E-01	5.783E-02	2.002E+06	0.130
$4f^3(4I)5d^2(3F)^6L_{11/2}$	$4f^3(4I)5d^5K6p^6L_{11/2}$	25373	3941.14	1.380E+00	1.063E-01	3.807E+06	0.033
$4f^3(4I)5d^2(3F)^6L_{11/2}$	$4f^3(4I)5d^5K6p^6I_{11/2}$	26882	3719.95	2.049E-01	1.673E-02	6.722E+05	0.041
$4f^3(4I)5d^2(3F)^6L_{11/2}$	$4f^3(4I)5d^5L6p^6K_{11/2}$	27650	3616.62	1.213E-01	1.018E-02	4.330E+05	0.069
$4f^3(4I)5d^2(3F)^6L_{11/2}$	$4f^3(4I)5d^5K6p^6I_{11/2}$	28842	3467.14	5.807E-02	5.088E-03	2.352E+05	0.351
$4f^3(4I)5d^2(3F)^6L_{11/2}$	$4f^3(4I)5d^5I6p^6K_{11/2}$	29386	3402.93	3.867E-01	3.452E-02	1.657E+06	0.120
$4f^3(4I)5d^2(3F)^6L_{11/2}$	$4f^3(4I)5d^3I6p^4K_{11/2}$	29450	3395.57	1.159E-02	1.037E-03	5.002E+04	0.124
$4f^3(4I)5d^2(3F)^6L_{11/2}$	$4f^3(4I)5d^5I6p^6K_{11/2}$	30233	3307.58	5.567E-02	5.112E-03	2.597E+05	0.164
$4f^3(4I)5d^2(3F)^6L_{11/2}$	$4f^3(4I)5d^3I6p^4H_{11/2}$	30410	3288.31	3.589E-02	3.316E-03	1.704E+05	0.320
$4f^3(4I)5d^2(3F)^6L_{11/2}$	$4f^3(4I)5d^5I6p^6I_{11/2}$	30982	3227.58	2.441E-04	2.297E-05	1.226E+03	0.999
$4f^3(4I)5d^2(3F)^6L_{11/2}$	$4f^3(4I)5d^5I6p^6I_{11/2}$	31155	3209.69	5.477E-02	5.184E-03	2.797E+05	0.186
$4f^3(4I)5d^2(3F)^6L_{11/2}$	$4f^3(4I)5d^5I6p^4K_{11/2}$	31541	3170.46	3.420E-02	3.276E-03	1.812E+05	0.373
$4f^3(4I)5d^2(3F)^6L_{11/2}$	$4f^3(4I)5d^5I6p^4H_{11/2}$	31848	3139.89	2.205E-04	2.133E-05	1.202E+03	0.541
$4f^3(4I)5d^2(3F)^6L_{11/2}$	$4f^3(4I)5d^3H6p^4I_{11/2}$	32432	3083.34	5.245E-03	5.167E-04	3.021E+04	0.319
$4f^3(4I)5d^2(3F)^6L_{11/2}$	$4f^3(4I)5d^5I6p^6H_{11/2}$	33244	3008.02	2.221E-03	2.242E-04	1.377E+04	0.427
$4f^3(4I)5d^2(3F)^6L_{11/2}$	$4f^3(4I)5d^5H6p^6H_{11/2}$	33332	3000.04	1.985E-05	2.010E-06	1.241E+02	0.938
$4f^3(4I)5d^2(3F)^6L_{11/2}$	$4f^3(4I)5d^5H6p^6G_{11/2}$	33384	2995.44	1.588E-04	1.611E-05	9.980E+02	0.446
$4f^3(4I)5d^2(3F)^6L_{11/2}$	$4f^3(4I)5d^5I6p^6I_{11/2}$	33499	2985.08	8.480E-04	8.629E-05	5.383E+03	0.424

NOTE— Table 10 is published in its entirety in the machine-readable format. Part of the values are shown here for guidance regarding its form and content.

- . 2007, *Relativistic Quantum Theory of Atoms and Molecules* (Springer, New York)
- Hotokezaka, K., Beniamini, P., & Piran, T. 2018, ArXiv e-prints, arXiv:1801.01141
- Jönsson, P., Gaigalas, G., Bieroń, J., Fischer, C. F., & Grant, I. 2013, *Computer Physics Communications*, 184, 2197
- Karp, A. H., Lasher, G., Chan, K. L., & Salpeter, E. E. 1977, *ApJ*, 214, 161
- Kasen, D., Badnell, N. R., & Barnes, J. 2013, *ApJ*, 774, 25
- Kasen, D., Fernández, R., & Metzger, B. D. 2015, *MNRAS*, 450, 1777
- Kasen, D., Metzger, B., Barnes, J., Quataert, E., & Ramirez-Ruiz, E. 2017, *Nature*, 551, 80
- Kasen, D., Thomas, R. C., & Nugent, P. 2006, *ApJ*, 651, 366
- Kasliwal, M. M., Nakar, E., Singer, L. P., et al. 2017, *Science*, 358, 1559
- Kilpatrick, C. D., Foley, R. J., Kasen, D., et al. 2017, *Science*, 358, 1583
- Kulkarni, S. R. 2005, arXiv:astro-ph/0510256, arXiv:astro-ph/0510256
- Li, L.-X., & Paczyński, B. 1998, *ApJL*, 507, L59
- Lipunov, V. M., Gorbvskoy, E., Kornilov, V. G., et al. 2017, *ApJL*, 850, L1
- McCully, C., Hiramatsu, D., Howell, D. A., et al. 2017, *ApJL*, 848, L32
- McKenzie, B., Grant, I., & Norrington, P. 1980, *Computer Physics Communications*, 21, 233
- Metzger, B. D. 2017, *Living Reviews in Relativity*, 20, 3
- Metzger, B. D., & Fernández, R. 2014, *MNRAS*, 441, 3444
- Metzger, B. D., Martínez-Pinedo, G., Darbha, S., et al. 2010, *MNRAS*, 406, 2650
- Nicholl, M., Berger, E., Kasen, D., et al. 2017, *ApJL*, 848, L18

Table 11. Energy levels (in cm^{-1}) relative to the ground state for the lowest states of Nd III.

No.	label	J	P	E
1	$4f^4({}^5I) {}^5I$	4	+	0.00
2	$4f^4({}^5I) {}^5I$	5	+	1072.58
3	$4f^4({}^5I) {}^5I$	6	+	2263.93
4	$4f^4({}^5I) {}^5I$	7	+	3542.92
5	$4f^4({}^5I) {}^5I$	8	+	4884.66
6	$4f^4({}^5F) {}^5F$	1	+	11739.04
7	$4f^4({}^5F) {}^5F$	2	+	12098.57
8	$4f^4({}^5F) {}^5F$	3	+	12724.33
9	$4f^4({}^5S) {}^5S$	2	+	13433.63
10	$4f^4({}^5F) {}^5F$	4	+	13459.96
11	$4f^4({}^5F) {}^5F$	5	+	14444.26
12	$4f^4({}^3K) {}^3K$	6	+	15065.97
13	$4f^3({}^4I)5d {}^5K$	5	-	15128.43
14	$4f^3({}^4I)5d {}^5L$	6	-	15257.69
15	$4f^4({}^3H) {}^3H$	4	+	16151.40
16	$4f^4({}^3K) {}^3K$	7	+	16180.31
17	$4f^3({}^4I)5d {}^5K$	6	-	16720.95
18	$4f^3({}^4I)5d {}^5L$	7	-	16985.08
19	$4f^4({}^5G) {}^5G$	2	+	17295.05
20	$4f^4({}^5G) {}^5G$	3	+	17368.09

NOTE— Table 11 is published in its entirety in the machine-readable format. Part of the values are shown here for guidance regarding its form and content.

- Olsen, J., Godefroid, M. R., Jönsson, P., Malmqvist, P. A., & Fischer, C. F. 1995, *Phys. Rev. E*, 52, 4499
- Perego, A., Radice, D., & Bernuzzi, S. 2017, *ApJL*, 850, L37
- Pian, E., D’Avanzo, P., Benetti, S., et al. 2017, *Nature*, 551, 67
- Radziemski, L. J., Fisher, K., & Steinhaus, D. 1970
- Rosswog, S. 2015, *International Journal of Modern Physics D*, 24, 1530012
- Rosswog, S., Sollerman, J., Feindt, U., et al. 2017, arXiv:1710.05445, arXiv:1710.05445
- Shappee, B. J., Simon, J. D., Drout, M. R., et al. 2017, *Science*, 358, 1574
- Shibata, M., Fujibayashi, S., Hotokezaka, K., et al. 2017, *PhRvD*, 96, 123012
- Siebert, M. R., Foley, R. J., Drout, M. R., et al. 2017, *ApJL*, 848, L26
- Smartt, S. J., Chen, T.-W., Jerkstrand, A., et al. 2017, *Nature*, 551, 75
- Soares-Santos, M., Holz, D. E., Annis, J., et al. 2017, *ApJL*, 848, L16
- Tanaka, M. 2016, *Advances in Astronomy*, 2016, 634197
- Tanaka, M., & Hotokezaka, K. 2013, *ApJ*, 775, 113
- Tanaka, M., Hotokezaka, K., Kyutoku, K., et al. 2014, *ApJ*, 780, 31
- Tanaka, M., Utsumi, Y., Mazzali, P. A., et al. 2017, *PASJ*, 69, 102
- Tanaka, M., Kato, D., Gaigalas, G., et al. 2018, *ApJ*, 852, 109
- Tanvir, N. R., Levan, A. J., González-Fernández, C., et al. 2017, *ApJL*, 848, L27
- Tominaga, N., Tanaka, M., Morokuma, T., et al. 2018, *PASJ*, arXiv:1710.05865

Table 12. Transition energies ΔE (in cm^{-1}), transition wavelengths λ (in \AA), line strengths S (in a.u.), weighted oscillator strengths gf and transition rates A (in s^{-1}) for E1 transitions of Nd III ion. All transition data are in length form. dT is the relative difference of the transition rates in length and velocity form as given by Eq. (5).

upper	lower	ΔE	λ	S	gf	A	dT
$4f^4(3P)3P_0$	$4f^3(4F)5d5D_1$	6521	15334.41	2.338E-03	4.632E-05	4.380E+02	0.948
$4f^4(3P)3P_0$	$4f^3(4F)5d3P_1$	9156	10920.99	1.996E-02	5.553E-04	1.035E+04	0.861
$4f^4(3P)3P_0$	$4f^3(4F)5d5P_1$	10206	9798.04	5.262E-03	1.631E-04	3.778E+03	0.787
$4f^4(3P)3P_0$	$4f^3(4F)5d5F_1$	10697	9348.19	8.930E-03	2.901E-04	7.382E+03	0.822
$4f^4(3P)3P_0$	$4f^3(4S)5d5D_1$	11516	8683.29	3.115E-05	1.090E-06	3.214E+01	0.890
$4f^4(3P)3P_0$	$4f^3(4S)5d3D_1$	12113	8255.57	1.272E-02	4.681E-04	1.527E+04	0.752
$4f^4(3P)3P_0$	$4f^3(4F)5d3D_1$	14250	7017.52	9.589E-02	4.150E-03	1.874E+05	0.710
$4f^4(3P)3P_0$	$4f^3(2G)5d3D_1$	17425	5738.84	7.686E-02	4.068E-03	2.746E+05	0.647
$4f^4(3P)3P_0$	$4f^3(4G)5d5F_1$	18400	5434.62	5.429E-04	3.034E-05	2.284E+03	0.634
$4f^4(3P)3P_0$	$4f^3(2P)5d3P_1$	19753	5062.36	1.351E-02	8.110E-04	7.036E+04	0.786
$4f^4(3P)3P_0$	$4f^3(4G)5d5D_1$	20499	4878.06	4.216E-03	2.625E-04	2.453E+04	0.562
$4f^4(3P)3P_0$	$4f^3(2D)5d3P_1$	20588	4857.14	6.608E-02	4.132E-03	3.894E+05	0.679
$4f^4(3P)3P_0$	$4f^3(2D)5d3S_1$	21850	4576.58	4.184E-02	2.777E-03	2.948E+05	0.711
$4f^4(3P)3P_0$	$4f^3(4F)6s5F_1$	22166	4511.37	1.708E-05	1.150E-06	1.257E+02	0.812
$4f^4(3P)3P_0$	$4f^3(2D)5d3S_1$	22582	4428.21	7.961E-03	5.461E-04	6.192E+04	0.707
$4f^4(3P)3P_0$	$4f^3(2P)5d3D_1$	23964	4172.76	1.943E-02	1.415E-03	1.806E+05	0.137
$4f^4(3P)3P_0$	$4f^3(4S)6s3S_1$	24808	4030.93	4.263E-04	3.213E-05	4.396E+03	0.318
$4f^4(3P)3P_0$	$4f^3(4S)6s3S_1$	25324	3948.70	3.464E-03	2.665E-04	3.800E+04	0.784
$4f^4(3P)3P_0$	$4f^3(2D)5d1P_1$	26223	3813.37	2.834E-03	2.257E-04	3.452E+04	0.389
$4f^4(3P)3P_0$	$4f^3(4D)5d5F_1$	27992	3572.45	4.279E-09	3.638E-10	6.339E-02	0.999

NOTE— Table 12 is published in its entirety in the machine-readable format. Part of the values are shown here for guidance regarding its form and content.

Troja, E., Piro, L., van Eerten, H., et al. 2017, *Nature*, 551, 71

Utsumi, Y., Tanaka, M., Tominaga, N., et al. 2017, *PASJ*, 69, 101

Valenti, S., David, Sand, J., et al. 2017, *ApJL*, 848, L24

Wollaeger, R. T., Korobkin, O., Fontes, C. J., et al. 2017, arXiv:1705.07084, arXiv:1705.07084

Wyart, J.-F. 2010, *Physica Scripta*, 82, 035302

Wyart, J.-F., Meftah, A., Bachelier, A., et al. 2006, *Journal of Physics B: Atomic, Molecular and Optical Physics*, 39, L77

Wyart, J.-F., Meftah, A., Sinzelle, J., et al. 2008, *Journal of Physics B: Atomic, Molecular and Optical Physics*, 41, 085001

Wyart, J.-F., Meftah, A., Tchang-Brillet, W.-. L., et al. 2007, *Journal of Physics B: Atomic, Molecular and Optical Physics*, 40, 3957

Yoca, S. E., & Quinet, P. 2014, *Journal of Physics B: Atomic, Molecular and Optical Physics*, 47, 035002

Zhang, Z. G., Svanberg, S., Palmeri, P., Quinet, P., & Biéumont, E. 2002, *A&A*, 385, 724

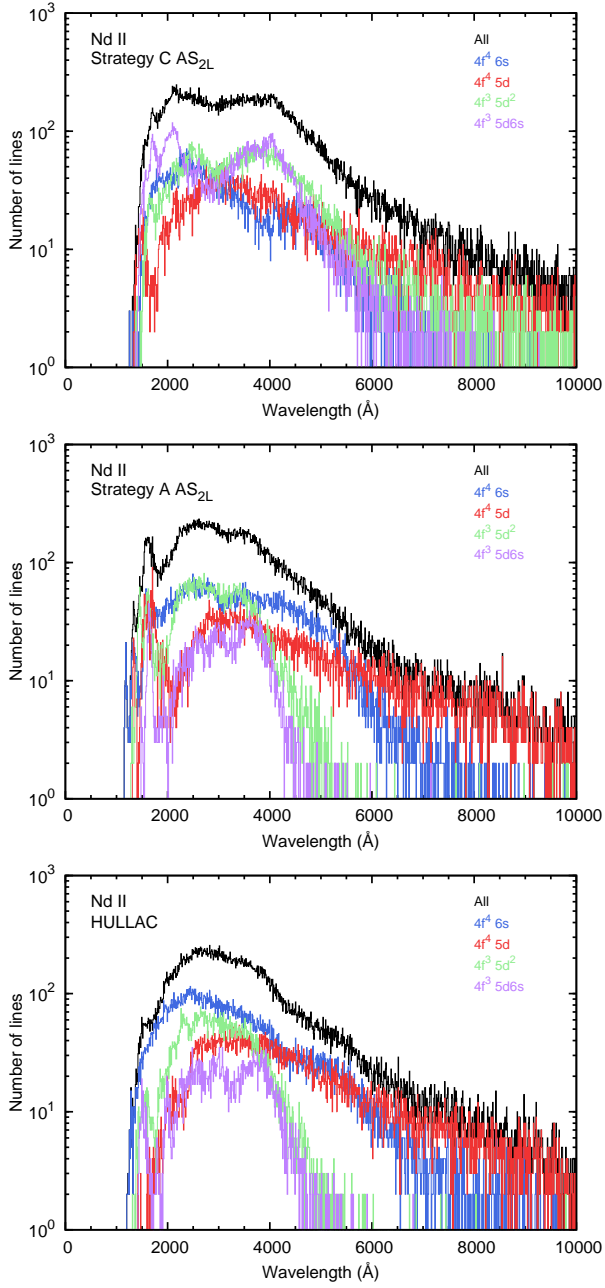


Figure 8. Number of strong transitions of Nd II as a function of wavelengths. The strong transitions are selected by the criterion of $g_i f_i \exp(-E_i/kT) > 10^{-5}$ with $T = 5000$ K. The black lines show total number of strong transitions while color lines show transitions from each lower-level configuration.

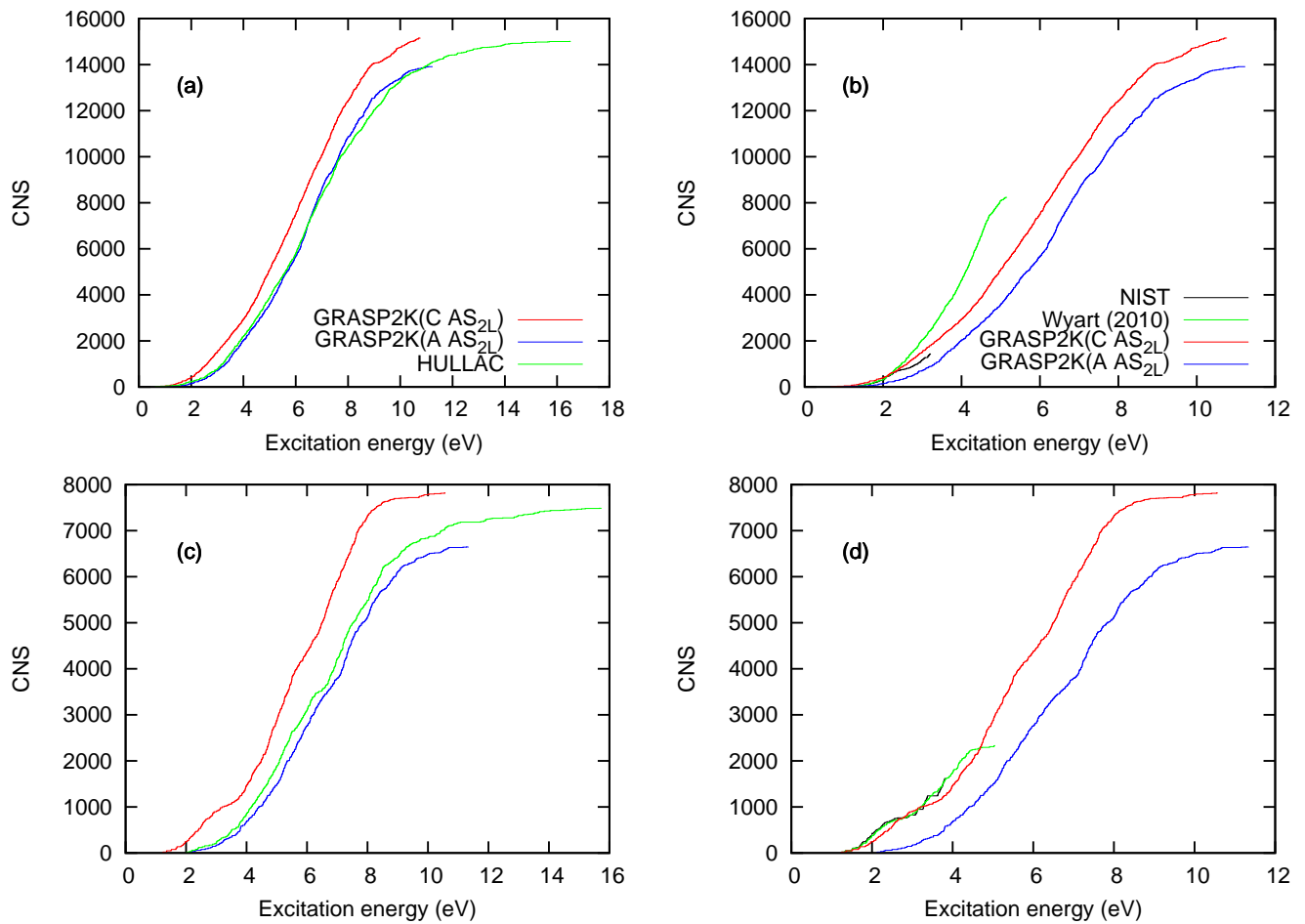


Figure 9. Cumulative number of states for $4f^3 5d^2$ (a,b) and $4f^3 5d 6s$ (c,d) configurations as a function of excitation energy. (a,c): Results with the present and previous GRASP2K and HULLAC calculations. (b,d): Results with the present GRASP2K calculation, NIST, and the semi-empirical method by Wyart (2010).

Table 13. Energy levels (in cm^{-1}) relative to the ground state for the lowest states of Nd IV.

No.	label	J	P	E
1	$4f^3({}^4I) {}^4I$	9/2	–	0.00
2	$4f^3({}^4I) {}^4I$	11/2	–	1748.59
3	$4f^3({}^4I) {}^4I$	13/2	–	3627.05
4	$4f^3({}^4I) {}^4I$	15/2	–	5595.78
5	$4f^3({}^4F) {}^4F$	3/2	–	13076.19
6	$4f^3({}^2H) {}^2H$	9/2	–	13536.44
7	$4f^3({}^4F) {}^4F$	5/2	–	14022.10
8	$4f^3({}^4S) {}^4S$	3/2	–	14617.16
9	$4f^3({}^4F) {}^4F$	7/2	–	14911.07
10	$4f^3({}^4F) {}^4F$	9/2	–	15979.23
11	$4f^3({}^2H) {}^2H$	11/2	–	16581.13
12	$4f^3({}^2G) {}^2G$	7/2	–	18780.28
13	$4f^3({}^4G) {}^4G$	5/2	–	19780.48
14	$4f^3({}^4G) {}^4G$	9/2	–	21211.00
15	$4f^3({}^4G) {}^4G$	7/2	–	21217.90
16	$4f^3({}^2K) {}^2K$	13/2	–	21444.78
17	$4f^3({}^4G) {}^4G$	9/2	–	22708.88
18	$4f^3({}^2D) {}^2D$	3/2	–	23160.03
19	$4f^3({}^2K) {}^2K$	15/2	–	23397.52
20	$4f^3({}^4G) {}^4G$	11/2	–	23768.32

NOTE— Table 13 is published in its entirety in the machine-readable format. Part of the values are shown here for guidance regarding its form and content.

Table 14. Transition energies ΔE (in cm^{-1}), transition wavelengths λ (in \AA), line strengths S (in a.u.), weighted oscillator strengths gf and transition rates A (in s^{-1}) for E1 transitions of Nd IV ion. All transition data are in length form. dT is the relative difference of the transition rates in length and velocity form as given by Eq. (5).

upper	lower	ΔE	λ	S	gf	A	dT
$4f^3(2P)5p^6\ ^2P_{1/2}$	$4f^2(3F)5p^65d\ ^2P_{1/2}$	52003	1922.95	3.607E-02	5.698E-03	5.140E+06	0.422
$4f^3(4D)5p^6\ ^4D_{1/2}$	$4f^2(3F)5p^65d\ ^2P_{1/2}$	44283	2258.20	7.141E-03	9.606E-04	6.283E+05	0.235
$4f^2(3F)5p^65d\ ^2P_{1/2}$	$4f^4(5F)5p^5\ ^6D_{1/2}$	83619	1195.89	3.829E-07	9.725E-08	2.268E+02	0.945
$4f^2(3F)5p^65d\ ^2P_{1/2}$	$4f^4(5G)5p^5\ ^6F_{1/2}$	85201	1173.69	2.099E-05	5.432E-06	1.315E+04	0.116
$4f^2(3F)5p^65d\ ^2P_{1/2}$	$4f^2(3F)5p^66p\ ^4D_{1/2}$	92307	1083.33	1.546E-05	4.336E-06	1.232E+04	0.249
$4f^2(3F)5p^65d\ ^2P_{1/2}$	$4f^4(3D)5p^5\ ^4P_{1/2}$	96617	1035.01	2.052E-05	6.022E-06	1.875E+04	0.739
$4f^2(3F)5p^65d\ ^2P_{1/2}$	$4f^4(3F)5p^5\ ^4D_{1/2}$	99613	1003.88	9.090E-05	2.750E-05	9.102E+04	0.448
$4f^2(3F)5p^65d\ ^2P_{1/2}$	$4f^4(3F)5p^5\ ^4D_{1/2}$	103718	964.15	2.294E-06	7.228E-07	2.593E+03	0.625
$4f^2(3F)5p^65d\ ^2P_{1/2}$	$4f^4(1D)5p^5\ ^2P_{1/2}$	105216	950.42	5.732E-04	1.832E-04	6.764E+05	0.229
$4f^2(3F)5p^65d\ ^2P_{1/2}$	$4f^2(1D)5p^66p\ ^2P_{1/2}$	108119	924.90	1.258E-02	4.132E-03	1.611E+07	0.069
$4f^2(3F)5p^65d\ ^2P_{1/2}$	$4f^4(5D)5p^5\ ^6D_{1/2}$	109048	917.03	6.412E-04	2.124E-04	8.424E+05	0.310
$4f^2(3F)5p^65d\ ^2P_{1/2}$	$4f^2(3P)5p^66p\ ^4D_{1/2}$	109666	911.85	4.762E-06	1.586E-06	6.363E+03	0.182
$4f^2(3F)5p^65d\ ^2P_{1/2}$	$4f^2(3P)5p^66p\ ^2S_{1/2}$	110081	908.41	5.629E-05	1.882E-05	7.608E+04	0.611
$4f^2(3F)5p^65d\ ^2P_{1/2}$	$4f^4(5D)5p^5\ ^6D_{1/2}$	110468	905.24	1.101E-03	3.695E-04	1.503E+06	0.170
$4f^2(3F)5p^65d\ ^2P_{1/2}$	$4f^4(3D)5p^5\ ^4D_{1/2}$	112421	889.51	1.612E-03	5.508E-04	2.321E+06	0.089
$4f^2(3F)5p^65d\ ^2P_{1/2}$	$4f^4(5S)5p^5\ ^4P_{1/2}$	113266	882.87	1.875E-04	6.451E-05	2.760E+05	0.153
$4f^2(3F)5p^65d\ ^2P_{1/2}$	$4f^2(3P)5p^66p\ ^4P_{1/2}$	115617	864.92	3.828E-03	1.344E-03	5.994E+06	0.192
$4f^2(3F)5p^65d\ ^2P_{1/2}$	$4f^4(2F)5p^5\ ^4D_{1/2}$	116976	854.87	6.502E-05	2.310E-05	1.054E+05	0.454
$4f^2(3F)5p^65d\ ^2P_{1/2}$	$4f^2(3P)5p^66p\ ^2P_{1/2}$	118179	846.17	3.156E-03	1.133E-03	5.277E+06	0.251
$4f^2(3F)5p^65d\ ^2P_{1/2}$	$4f^4(2P)5p^5\ ^4P_{1/2}$	119038	840.07	5.618E-03	2.031E-03	9.600E+06	0.113

NOTE— Table 14 is published in its entirety in the machine-readable format. Part of the values are shown here for guidance regarding its form and content.